the FEBS Journal

Degradation of nuclear DNA by DNase II-like acid DNase in cortical fiber cells of mouse eye lens

Masaki Nakahara[1], Akiomi Nagasaka[2], Masato Koike[3], Kaori Uchida[1], Kohki Kawane[1,2], Yasuo Uchiyama[3] and Shigekazu Nagata[1,2,4]

1 Department of Genetics, Osaka University Medical School, Japan
2 Laboratory of Genetics, Integrated Biology Laboratories, Graduate School of Frontier Biosciences, Osaka University, Japan
3 Department of Cell Biology and Neuroscience, Osaka University Medical School, Japan
4 Solution Oriented Research for Science and Technology, Japan Science and Technology Corporation, Osaka, Japan

Keywords
acid DNase; differentiation; eye lens; gene array; lysosome

Correspondence
S. Nagata, Department of Medical Chemistry, Graduate School of Medicine, Kyoto University, Yoshida, Sakyo-ku, Kyoto 606-8501, Japan
Fax: +81 75 753 9446
Tel: +81 75 753 9441
E-mail: snagata@mfour.med.kyoto-u.ac.jp
Website: http://www.med.osaka-u.ac.jp/pub/genetic/English%20Site/HP%20top%89p%8c%ea/Home%20top%20en.html

(Received 28 February 2007, revised 9 April 2007, accepted 17 April 2007)

doi:10.1111/j.1742-4658.2007.05836.x

The eye lens is composed of fiber cells that differentiate from epithelial cells on its anterior surface. In concert with this differentiation, a set of proteins essential for lens function is synthesized, and the cellular organelles are degraded. DNase II-like acid DNase, also called DNase IIβ, is specifically expressed in the lens, and degrades the DNA in the lens fiber cells. Here we report that DNase II-like acid DNase is synthesized as a precursor with a signal sequence, and is localized to lysosomes. DNase II-like acid DNase mRNA was found in cortical fiber cells but not epithelial cells, indicating that its expression is induced during the differentiation of epithelial cells into fiber cells. Immunohistochemical and immunocytochemical analyses indicated that DNase II-like acid DNase was colocalized with Lamp-1 in the lysosomes of fiber cells in a relatively narrow region bordering the organelle-free zone, and was often found in degenerating nuclei. A comparison by microarray analysis of the gene expression profiles between epithelial and cortical fiber cells of young mouse lens indicated that some genes for lysosomal enzymes (cathepsins and lipases) were strongly expressed in the fiber cells. These results suggest that the lysosomal system plays a role in the degradation of cellular organelles during lens cell differentiation.

The lens is an avascular tissue that focuses light onto the retina in the eye. It consists of closely packed fiber cells that are bounded at the anterior by a monolayer of epithelial cells. Fiber cells are produced continuously by the differentiation of the epithelial cells near the lens equator. New fiber cells are added steadily, and as there is no cell turnover, the lens grows throughout life [1,2]. The differentiating fiber cells are overlaid by new layers of younger cells, and when they have fully differentiated, the fiber cells are incorporated as part of the lens nucleus. As the epithelial cells differentiate into fiber cells, they change morphologically to become fiber-like, and they synthesize lens-specific proteins such as crystallins. One of the most notable changes is the elimination of all organelles, including the endoplasmic reticulum, mitochondria, Golgi apparatus, and nucleus, at the last stage of differentiation [3]. The adult lens thus contains two populations of fiber cells in the cortex: a cortical layer of differentiating fiber cells, which contain organelles, and the non-nucleated fiber cells, which do not contain organelles. Several degradation mechanisms have been proposed, most prominently apoptosis [4], cytosolic degradation [5], and autophagy [6,7]. However, the mechanism that operates during the differentiation of fiber cells has been very elusive.

In mammals, there are two acid DNases, DNase II and DNase II-like acid DNase (DLAD) or DNase IIβ [8–10]. DNase II is ubiquitously expressed in various tissues, particularly in macrophages [11,12]. The

Abbreviations
DLAD, DNase II-like acid DNase; rDLAD, recombinant DNase II-like acid DNase.

DNase II expressed in macrophages is responsible for degrading the DNA of apoptotic cells and the nuclei expelled from erythroid precursor cells [13,14]. In contrast, DLAD is uniquely expressed in the eye lens [15]. The targeted mutation of the *DLAD* gene in mice causes cataract of the nucleus lentis [15] from a large amount of naked DNA that accumulates in the cytoplasm of the differentiated fiber cells, indicating that DLAD is responsible for cell-autonomously digesting its own chromosomal DNA in lens fiber cells during lens cell differentiation.

In this study, we found that the expression of mouse DLAD is strongly induced during lens fiber cell differentiation. DLAD resides in the lysosomes of cortical fiber cells, close to the organelle-free zone. Small lysosomal vacuoles carrying DLAD were present surrounding nuclei, and degenerating nuclei were localized with DLAD. In addition to DLAD, a set of lysosomal enzymes was strongly upregulated in the cortical fiber cells, suggesting an involvement of lysosomes in degradation of organelles during lens cell differentiation.

Results

Localization of DLAD to lysosomes

DLAD was identified as a protein homologous to DNase II [9,10]. An alignment of the amino acid sequence of murine DLAD with that of murine DNase II (Fig. 1A) showed 37.9% identity at the amino acid sequence level. In particular, three histidine residues that are necessary for the DNase activity of porcine DNase II [16] and their flanking regions were well conserved. There is some controversy about the subunit structure of DNase II [17,18]: the DNase II from porcine spleen is reported to be composed of three subunits (α_1, α_2 and β) [18], whereas human DNase II is proposed to be a single polypeptide with a clipped signal peptide [17]. To determine the subunit structure of murine DLAD and DNase II, they were tagged with Flag at the C-terminus, synthesized in human 293T cells, and purified to homogeneity. Both the purified recombinant DLAD and DNase II were composed of a single polypeptide (Fig. 1B). An Edman degradation analysis for N-terminal amino acids indicated that mouse DLAD and DNase II start from Thr1 and Leu1, respectively, leaving signal sequences of 22 and 19 amino acids, respectively (Fig. 1A). These cleavage sites conform to von Heijne's criteria for signal sequences, and the overall structures of mouse DLAD and DNase II are consistent with that proposed for human DNase II [17]. As shown for human DLAD [10], mature murine DLAD is a basic protein with a pI of 9.56, which contrasts with murine DNase II's pI of 7.2. As reported for DNase II [19], mouse DLAD is a glycoprotein, because treatment of rDLAD with *N*-glycosidase reduced its molecular mass from 67 to 40 kDa (data not shown).

Proteins carrying a signal sequence can be secreted from cells or imported into lysosomes. To determine whether DLAD is secreted or kept inside the cells, the DLAD expression plasmid was introduced into 293T cells, and the DLAD protein levels in the culture supernatant and cells were analyzed by western blotting. As shown in Fig. 1C, compared with mouse DNase II, which could be efficiently secreted into the culture supernatant, mouse DLAD was mainly found in the cell lysates. HeLa cell transformants expressing mouse DLAD were then established, and stained with a mAb to mouse DLAD. As shown in Fig. 1D, very strong staining with granular signals was found adjacent to the nucleus. The parental HeLa cells were not stained with the mAb, confirming its specificity. Signals from an antibody to Lamp-1, a lysosomal membrane protein, colocalized with the anti-DLAD signals, confirming that DLAD could be present in lysosomes.

Expression of DLAD in lens cortical fiber cells

During the differentiation of lens epithelial cells into fiber cells, the gene expression profile greatly changes [20]. An RT-PCR analysis of RNA from epithelial and fiber cells indicated that E-cadherin, a marker protein for epithelial cells [21], was expressed in lens epithelial cells, but was almost completely downregulated in the fiber cells (Fig. 2A). On the other hand, gene expression for crystallin γD, which is needed to maintain the transparency of the lens, was strongly activated in the fiber cells. Filensin, an eye-specific intermediate filament, was also expressed only in fiber cells. DLAD is necessary to degrade nuclei in the lens fiber cells [15]. Accordingly, a western blotting analysis of the epithelial and cortical fiber cells indicated that the cortical fiber cells but not epithelial cells expressed a DLAD protein of about 50 kDa (Fig. 2B). This specific expression of DLAD in the cortical fiber cells could also be observed at the RNA level. That is, northern hybridization with DLAD cRNA showed a major band of 1.8 kb and a minor band of 4.0 kb in the RNA from cortical fiber cells but not from epithelial cells (Fig. 2B). The size of the minor band was consistent with it being a DLAD precursor RNA carrying introns. A real-time PCR analysis indicated that the DLAD mRNA level in the cortical fiber cells was 17 times higher than in epithelial cells (Fig. 2B).

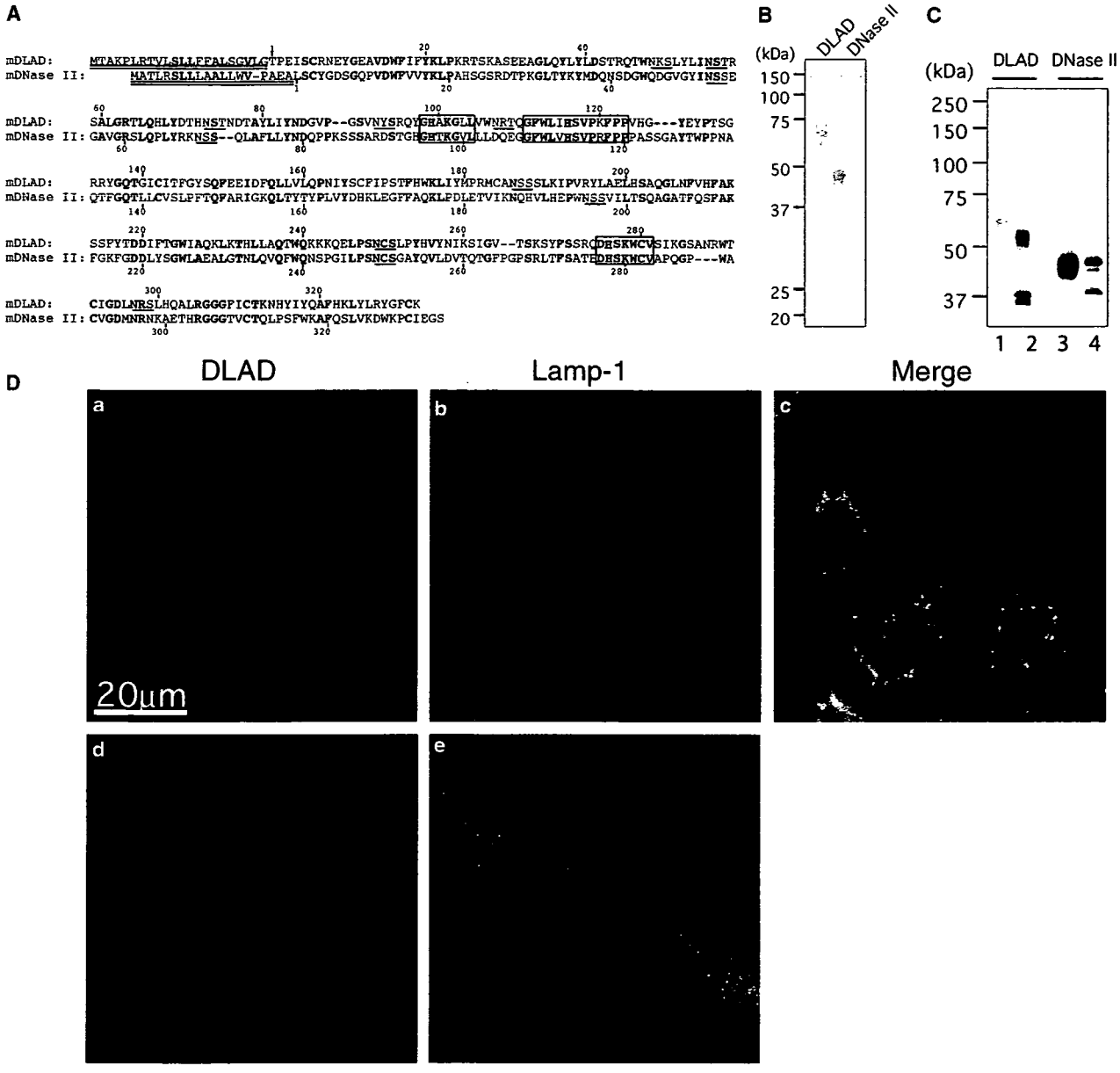

Fig. 1. Localization of murine DLAD to lysosomes. (A) Alignment of mouse DLAD and DNase II amino acid sequences. The amino acid sequences of mouse DLAD and DNase II were aligned to give maximum homology by introducing several gaps (–) using GENETYX-MAC genetic information-processing software (version 12) (Genetyx, Tokyo, Japan).The amino acid residues conserved between the two proteins are shown in bold. The amino acids are numbered from the N-terminus, which was determined by Edman degradation of mature rDLAD and rDNase II. The signal sequences are marked by double underlines. Putative active sites carrying the conserved histidine residues (red) are boxed. Potential N-glycosylation sites (Asn-X-Ser/Thr) are underlined. (B) Production of mouse rDLAD and rDNase II. Mouse rDLAD and rDNase II were produced in human 293T cells transfected with their respective expression plasmid. The DLAD and DNase II secreted into the culture medium were purified, and 0.5 μg of protein was subjected to SDS/PAGE followed by staining with Coomassie Brilliant Blue. The molecular masses of standard proteins are shown in kDa on the left. (C) Transient expression of rDLAD and rDNase II in 293T cells. Human 293T cells were transfected with the expression vector for Flag-tagged DLAD or DNase II, and cultured for 2 days. The culture supernatants were collected, and the cells were lysed. The Flag-tagged recombinant proteins in the culture supernatants were immunoprecipitated with anti-(Flag) protein A–sepharose. Aliquots of the immunoprecipitates (lanes 1 and 3) and cell lysates (lanes 2 and 4) corresponding to 5×10^4 cells were separated by SDS/PAGE (10%), followed by western blotting with the antibody to Flag. (D) Stable expression of DLAD in HeLa cells. Human HeLa cells were stably transformed with the mouse DLAD expression plasmid. The parental HeLa cells (d, e) or their transformants (a, b, c) were stained with hamster mAb to mouse DLAD (a, d; red) or mouse mAb to human Lamp-1 (b, e; green). In (c), the images obtained with anti-DLAD and anti-Lamp-1 are merged. Scale bar: 20 μm.

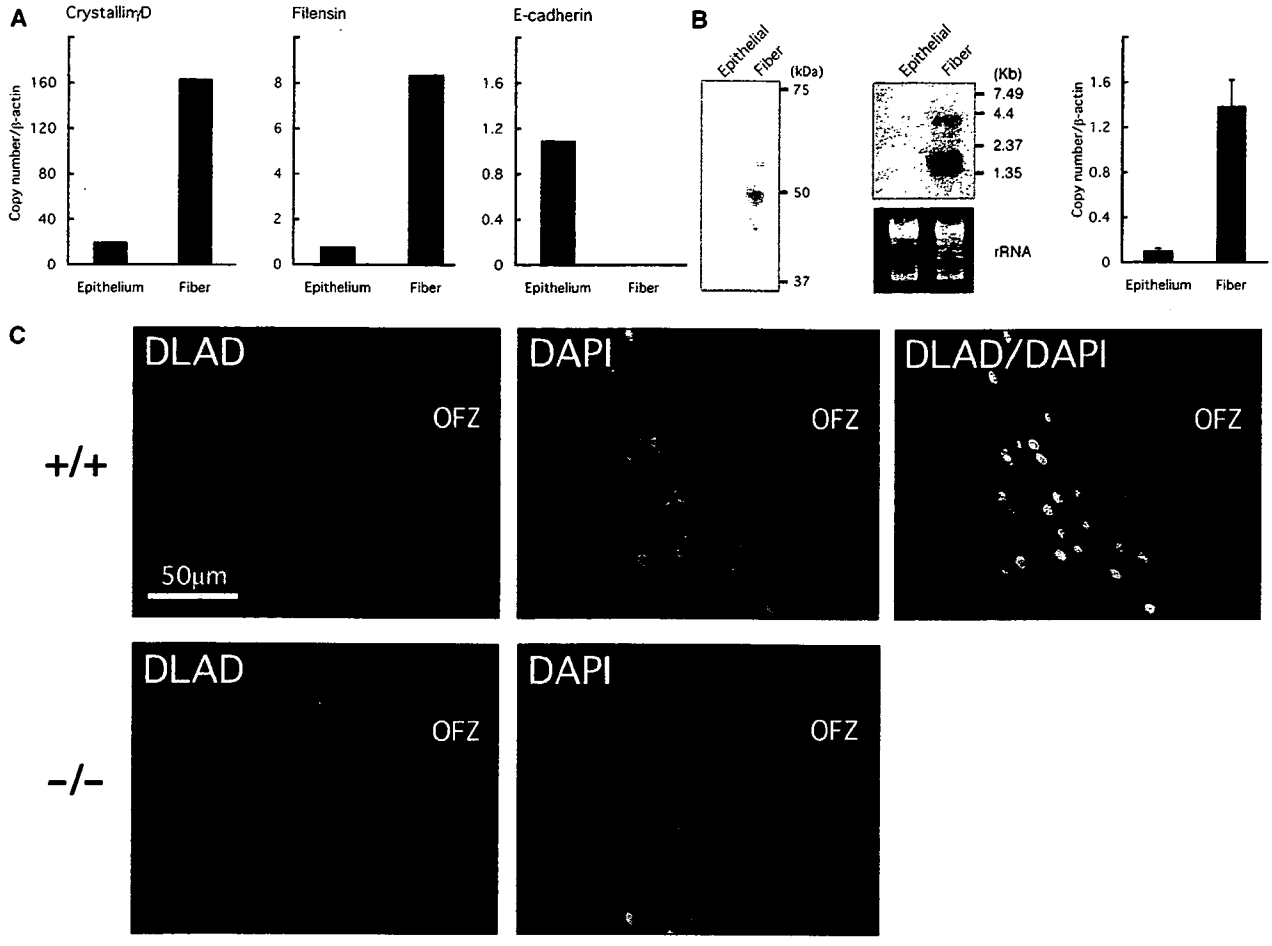

Fig. 2. Expression of DLAD in lens cortical fiber cells. (A) Different gene expression between epithelial cells and fiber cells in the lens. The mRNA levels for crystallin γD, filensin and E-cadherin in lens epithelial and fiber cells were determined by real-time PCR. As an internal control, the level for actin mRNA was determined, and the mRNA expression levels for crystallin γD, filensin and E-cadherin were expressed as ratio to actin mRNA. Experiments were performed in duplicate, and the average values are shown. (B) Specific expression of DLAD in lens fiber cells. Left panel: cell lysates (7.5 μg of protein) prepared from the epithelial (Epithelial) or cortical fiber (Fiber) cells of mouse eye lens were subjected to western blot analysis with the mAb to DLAD. The sizes of standard proteins are shown in kDa on the right. Middle panel: total RNA (1.0 μg) prepared from the lens epithelial or fiber cells was analyzed by northern hybridization using mouse DLAD cRNA as the probe. The sizes of the marker RNAs are shown in kb on the right. The lower panel shows a gel stained with SYBR Gold Nucleic Acid Gel Stain (Molecular Probe) for rRNA. Right panel: DLAD mRNA levels in epithelial and fiber cells were determined by real-time PCR, and the expression levels are shown as ratios to that of actin mRNA. The experiment was performed three times, and average values are plotted with SD (bars). (C) Localization of DLAD in mouse eye lens. Midsagittal lens slices from $DLAD^{+/+}$(+/+) or $DLAD^{-/-}$ (−/−) mice were stained with the mAb to DLAD (red), and this was followed by DAPI staining (blue). Scale bar: 50 μm. OFZ, organelle-free zone.

We then used immunohistochemistry to locate DLAD expression in the mouse lens. As shown in Fig. 2C, strong signals for DLAD were observed only in the layers of cortical fiber cells that surround the organelle-free zone. The signals were not detected in sections from $DLAD^{-/-}$ lens, verifying the authenticity of this result. These results indicated that the *DLAD* gene is transiently activated at the final stage of lens cell differentiation, and the expressed DLAD protein is degraded immediately after the organelles are destroyed. The lens sections were then costained for DLAD and Lamp-1, and analyzed by light and electron microscopy. As shown in Fig. 3A, Lamp-1 was ubiquitously expressed in the lens fiber cells, which contrasts with the limited expression of DLAD in the fiber cell layers adjacent to the organelle-free zone. The immunoelectron microscopy showed prominent signals for Lamp-1 in the lysosomes of fiber cell in the cortical zones, where the signals for DLAD were not frequent (Fig. 3Ba,b). On the other hand, the DLAD signals could be frequently detected in the fiber cell layers close to the organelle-free zone, and were colocalized to lysosomes

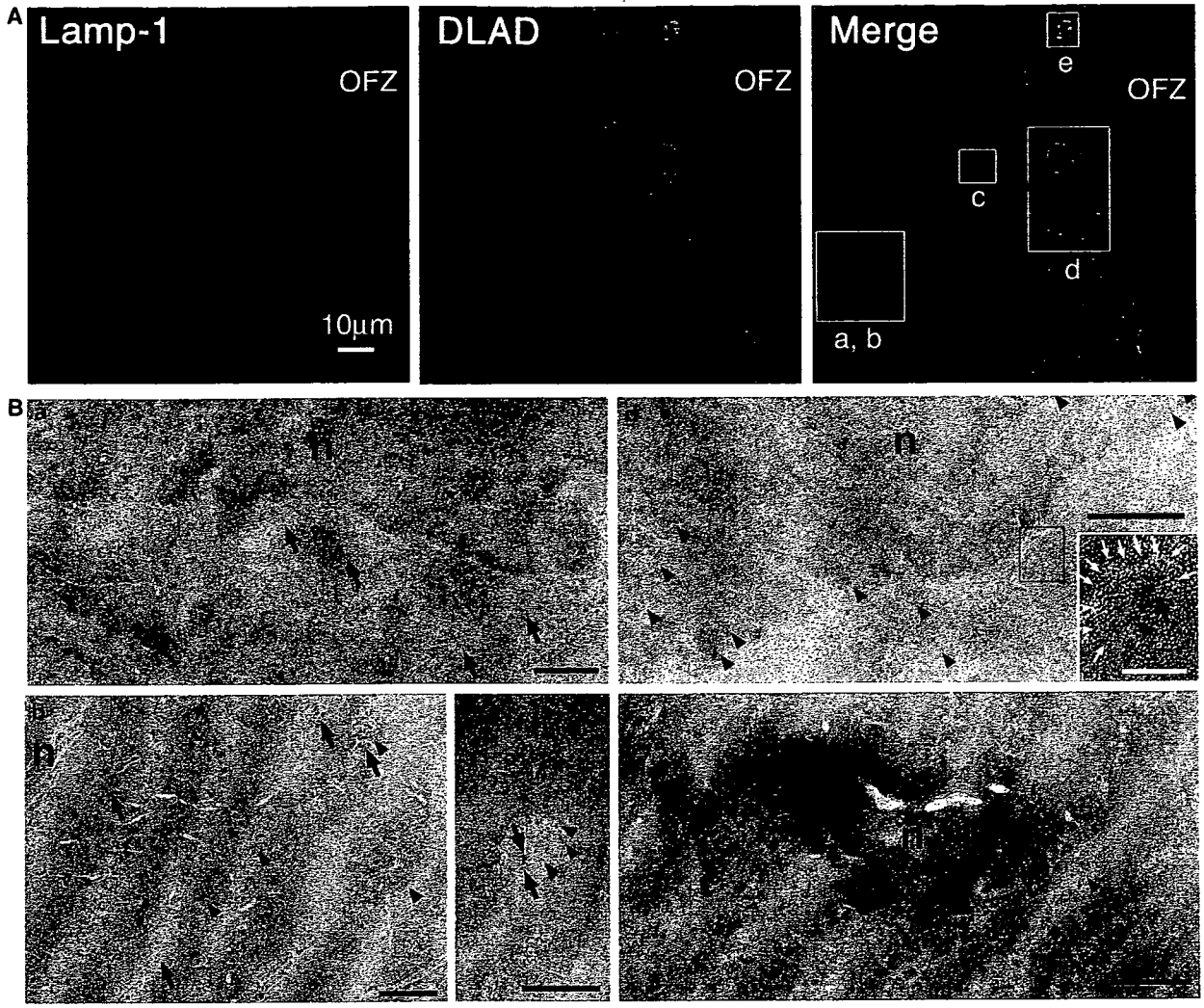

Fig. 3. Immunohistochemical and immunocytochemical staining for Lamp-1 and DLAD in mouse lens fiber cells. (A) Immunohistochemical staining. Lenses from 6-day-old mice were stained with Lamp-1 (red, left panel) and DLAD (green, middle panel). In the right panel, the staining profiles for Lamp-1, DLAD and DAPI are merged. OFZ, organelle-free zone. Scale bar: 10 μm. The fields analyzed by electron microscopy are indicated. (B) Immunocytochemical staining. The thin cryosections from the fields indicated in (A) were stained for Lamp-1 (10 nm gold particles, arrows) and DLAD (5 nm gold particles, arrowheads). n, nucleus. Scale bars: 0.25 μm. In (d), the boxed area is enlarged in the inset. White arrows indicate membranous structure. The scale bar in the inset is 0.1 μm.

together with Lamp-1 (Fig. 3Bc,d). Lysosomes carrying DLAD in this region were relatively small and associated with nuclei, and many DLAD-specific signals were found scattered in the nuclei (Fig. 3A,Bd). In particular, the degenerating nuclei carried DLAD (Fig. 3Be). These results suggested that DLAD is transferred from lysosomes to nuclei to degrade DNA.

Expression of other lysosomal enzymes in cortical fiber cells

To examine whether other enzymes and factors were induced during fiber cell differentiation, the gene expression profiles of the epithelial and fiber cells were compared by gene array analysis. The expression of about 500 genes was upregulated more than five-fold in the fiber cells, and a similar number of genes was downregulated at least five-fold. Major upregulated genes were the crystallins, ion transporters, and sugar transporters, as well as transcription factors that may regulate the differentiation of fiber cells (GEO GSE7533). In addition, several lysosomal hydrolases were strongly upregulated in the fiber cells (Table 1). That is, the mRNA levels for lysosomal proteases such as cathepsin G, cathepsin R and legumain were 5–25 times higher in fiber cells than in epithelial cells. A

Table 1. Hydrolases and their related genes upregulated in the lens fiber cells. Gene array analysis was performed using a Codelink Bioarray System. Signals were obtained by dividing the raw hybridization data by the median value. The median values were 25.0 and 7.7 for the epithelial and fiber cell RNAs, respectively. The increase in gene expression (Fold increase) was determined by dividing the signal obtained with fiber cell RNA by the signal obtained with epithelial cell RNA, and is shown as the fold increase.

Gene	Epithelial cell signal	Fiber cell signal	Fold increase
DNase II-like acid DNase (*dlad* or *dnase2b*)	3.3	28.4	8.6
Cathepsin G (*ctsg*)	9.3	50.6	5.4
Cathepsin R (*ctsr*)	0.6	16.2	24.7
Cathepsin J (*ctsJ*)	0.5	6.3	10.9
Legumain (*lgmn*)	3.9	27.7	7.1
Pancreatic lipase-related protein 2 (*pnliprp2*)	18.4	1400.7	76.3
Phospholipase a2, group vii (*pla2g7*)	1.0	79.7	78.4
Fatty acid-binding protein 5 (*fabp5*)	218.5	3014.9	13.8
Autophagy atg3p/aut1p-like (*atg3*)	15.2	112.7	7.4
Autophagin-1 (*atg4b*)	13.5	65.5	4.8
Caspase 7 (*casp7*)	5.7	58.8	10.9

specific lipase (pancreatic lipase-related protein 2) and a phospholipase (phospholipase a2, group vii) were also strongly upregulated in the lens fiber cells, suggesting that these enzymes are involved in degrading cellular organelles in the fiber cells. In this regard, it is noteworthy that the expression of some proteins involved in autophagy (atg3 and atg4b) was significantly (five- to eight-fold) upregulated in the fiber cells.

Discussion

The removal of cellular organelles during differentiation of fiber cells in the lens is essential to maintain the transparency of the eye lens, and a defect in this process can lead to cataract formation [15]. Among many models proposed for organelle degradation in the lens, three models (apoptosis, cytosolic degradation, and autophagy) predominate [4–7]. That is, when fiber cells differentiate, they undergo a series of morphologic and biochemical changes (condensation and fragmentation of chromatin, and generation of TdT-mediated dUTP-biotin nick end labeling (TUNEL)-positive DNA fragments) that are similar to those found in apoptotic cells [22]. Findings including the temporal activation of caspase-like activities [23], the degradation of some canonical caspase substrates [24] and the downregulation of antiapoptotic Bcl-2 members [25] in differentiating fiber cells also supported the idea of apoptosis being involved in lens cell differentiation. On the other hand, caspase-activated DNase, which is responsible for the apoptotic DNA fragmentation [26], is not expressed in lens fiber cells, and there is no abnormality in the lens of mice deficient in caspase-activated DNase [15]. Moreover, Zandy *et al.* [27] recently reported that the organelle-free zone is correctly formed in the eye lens of mice lacking caspase 3, caspase 6, or both, indicating that the elimination of fiber cell organelles does not require apoptosis or a caspase-dependent process. However, the expression of caspase 7 specifically increases in the fiber cells (Table 1), and some caspase 3-deficient mice transiently develop cataracts [27]. Therefore, it is possible that some caspases may regulate the development of the eye lens.

In the model in which organelles undergo cytosolic degradation, 15-lipoxygenase integrates into organelle membranes, permeabilizing the organelles to create access for cytosolic proteolytic machinery, such as the ubiquitin–proteasome system [28]. As 15-lipoxygenase was found in differentiating fiber cells, van Leyen *et al.* [5] proposed the involvement of lipoxygenase-mediated cytosolic degradation in programmed organelle degradation in the eye lens. However, the expression levels of 15-lipoxygenase and 12-lipoxygenase determined by our gene array analysis were comparable between epithelial and fiber cells. Furthermore, expression of proteases in the ubiquitin-dependent degradation system was not activated during differentiation into fiber cells, suggesting that the cytosolic degradation system may not be involved in the removal of organelles during lens cell differentiation. No lens abnormality was reported in mice deficient in 15-lipoxygenase or 12-lipoxygenase [29,30], supporting this idea.

We previously reported that DLAD is specifically expressed in the eye lens, and the null mutation of *DLAD* causes cataract due to the accumulation of undigested DNA in the cytoplasm of fiber cells [15]. The nuclei of the fiber cells are degraded in the fiber cell layers near the organelle-free zone. Consistent with this finding, DLAD mRNA was more abundant in

fiber cells than in epithelial cells, and the DLAD protein was found frequently in the few layers of fiber cells adjacent to the organelle-free zone, indicating that the expression of DLAD is tightly coupled with the differentiation of fiber cells. This finding agrees with results from mice deficient in the transcription factor Foxe3, which have a defect in the differentiation of lens cells; they do not express DLAD, and cannot degrade nuclei in the fiber cells [31]. As DLAD is related to DNase II, which works best in the acidic conditions in lysosomes, we previously postulated that DLAD also functions in lysosomes [15]. Here, we found that nuclei were associated with lysosomes in the last stage of fiber cell differentiation, and DLAD was often localized to degenerating nuclei in the fiber cells. These results suggest that the nuclei are fused with lysosomes and that DLAD digests the chromosomal DNA. Nuclei have a double membrane. Simple fusion of lysosomes to nuclei will bring the lysosomal enzymes to the lumen of the nuclear envelope but not the nucleoplasm. In the case of SV40, in which the SV40 genome should be transported from the endoplasmic reticulum to nuclei, a newly formed channel in the nuclear membrane seems to be responsible for this transport [32]. It may be possible that a similar mechanism operates to transport lysosomal enzymes into the nucleus in the lens fiber cells.

Hawse *et al.* [20] recently analyzed the gene expression profiles of epithelial and fiber cells in the human lens, and noticed global gene expression differences between them. However, probably due to the aged lens (average age greater than 56 years) that were analyzed, their analysis did not clearly indicate the genes that are involved in the degradation of organelles. We used here the mouse lens at postnatal day 13, when the differentiation of epithelial cells to fiber cells actively takes place [1], and found increased expression of lysosomal enzymes in fiber cells. This suggests that lysosomes are involved in the degradation of organelles during fiber cell differentiation. Genes for Atg3 and Atg4b for autophagy [33], and fatty acid binding protein 5, which is involved in lipid transport [34], were also activated in fiber cells (Table 1). These results and the observation of organelle degradation within autophagic vacuoles in the differentiating fiber cells [6] support the idea that organelles in the lens fiber cells are degraded by lysosomal enzymes. On the other hand, Matsui *et al.* [35] recently reported that there is no abnormality in lens cell differentiation in mice lacking Atg5, a protein essential for autophagosome formation, suggesting that the canonical autophagic mechanism is not involved in this process. It will be necessary to determine whether the lysosomal enzymes upregulated in fiber cells are in fact involved in degradation of organelles during fiber cell differentiation. Learning how nuclei and other organelles are degraded by lysosomal enzymes will be a future challenge to increase our understanding of lens cell differentiation, and its abnormality in cataract formation.

Experimental procedures

Mice and cell lines

C57BL/6 mice were purchased from Japan SLC (Shizuoka, Japan). The $DLAD^{-/-}$ mice have been described previously [15]. All animal experiments were carried out in accord with protocols approved by the Osaka University Medical School Animal Care and Use Committee. HeLa cells were maintained in DMEM containing 10% fetal bovine serum (GibcoBRL, Gaithersburg, MD). To establish HeLa cell transformants expressing DLAD, mouse DLAD cDNA was tagged with Flag at the C-terminus and inserted into pEF-BOS-EX [36] to generate pEF-DLAD-Flag. HeLa cells were cotransfected with pEF-DLAD-Flag and pSTneoB carrying the neomycin resistance gene, and the G-418-resistant transformants expressing mouse DLAD were identified by western blotting.

Recombinant DLAD, monoclonal antibody, and analysis of N-terminal amino acid

Recombinant (r)DLAD and DNase II were produced by transfecting human 293T cells (ATCC CRL-11268) with pEF-DLAD-Flag or pEF-DNase II-Flag, and the protein secreted into the medium was purified to homogeneity using the anti-Flag M2 affinity gel (Sigma, St Louis, MO).

To produce monoclonal antibodies against DLAD, Armenian hamsters were immunized with rDLAD. Lymphocytes from the inguinal and popliteal lymph nodes were fused with $NSO^{bcl\text{-}2}$ mouse myeloma [37], and hybridomas were screened by ELISA for the ability to bind DLAD. Of the positive clones, clone 6-6-1 was suitable for immunohistochemistry and clone 16-2-5 for western blotting and immunohistochemistry.

The N-terminal amino acid of rDLAD and DNase II was determined by Edman degradation as a custom service at APRO Life Science Institute (Naruto, Japan).

Western blot

To prepare lens epithelial and cortical fiber cells, lenses from 13-day-old mice were soaked in Hank's balanced salt solution containing 1.26 mM $CaCl_2$ and 0.91 mM $MgCl_2$, and dissected by forceps into capsules that included the adhering epithelial cells and into cortical fiber cells. The capsules and cortical fiber cells were homogenized in

50 mM Pipes buffer (pH 7.4) containing 50 mM KCl, 2 mM $MgCl_2$, 5 mM EGTA, 1 mM dithiothreitol, 200 mM sorbitol, 20 mM cytochalasin B, 1 mM pepstatin A, and a mixture of protease inhibitors (Complete; Roche Diagnostic, Basel, Switzerland), and centrifuged at 500 *g* for 5 min using an MX-150 centrifuge (TOMY, Tokyo, Japan) with a TMP-II rotor (TOMY). For western blotting, the cell lysates were fractionated by electrophoresis on a 10% polyacrylamide gel (Bio Craft, Tokyo, Japan), and transferred to a membrane (Immobilon-P; Millipore, Bedford, MA). The membranes were probed with 1.5–3.0 $\mu g \cdot mL^{-1}$ hamster mAb to mouse DLAD (clone 16-2-5), followed by 10 000-fold diluted peroxidase-conjugated protein A (Bio-Rad Laboratories, Hercules, CA). The bands were revealed by chemiluminescence using a SuperSignal West Femto Maximum Sensitivity Substrate kit (Pierce Chemical, Rockford, IL).

Immunohistochemistry

HeLa cell transformants expressing DLAD were grown in Laboratory-Tek II chamber slides (Nalge Nunc, Rochester, NY), and fixed with cold acetone. After blocking of nonspecific binding sites with NaCl/P_i containing 5% goat serum and 1% BSA, the cells were incubated for 60 min with 10 $\mu g \cdot mL^{-1}$ of biotinylated mAb to DLAD (clone 6-6-1) and mouse mAb to Lamp-1 (clone H4A3; Santa Cruz Biotechnology, Santa Cruz, CA). This was followed by staining for 30 min with 3.7 $\mu g \cdot mL^{-1}$ Cy3-conjugated streptavidin (Sigma) and 10 $\mu g \cdot mL^{-1}$ Alexa Fluor 488-conjugated anti-(mouse IgG) (Molecular Probes, Carlsbad, CA). The cells were mounted with FluorSave (Calbiochem, San Diego, CA), and observed by confocal fluorescence microscopy (LMS510; Carl Zeiss MicroImaging, Thornwood, NY). For mouse lenses, lenses from mice 6 to 13 days old were fixed for 2 h at 4 °C with 4% paraformaldehyde in 0.1 M phosphate buffer (pH 7.4), successively immersed for 12 h per step in 0.1 M phosphate buffer (pH 7.4) containing 10%, 15% or 20% sucrose, embedded in OCT compound (Sakura Finetek, Tokyo, Japan), and cut into slices of 4 or 10 μm. The sections were postfixed for 10 min with methanol, treated for 15 min with 0.1% Triton in NaCl/P_i, and incubated for 60 min in NaCl/P_i containing 5% goat serum and 1% BSA. They were stained with 2 $\mu g \cdot mL^{-1}$ hamster mAb to DLAD (clone 16-2-5) and rat anti-Lamp-1 (clone 1D4B; Santa Cruz Biotechnology). Cy3-conjugated (Jackson Immunoresearch Laboratories, West Grove, PA) or Alexa Fluor 488-conjugated goat anti-(hamster IgG) (Invitrogen, Carlsbad, CA) and Alexa Fluor 594-conjugated anti-(rat IgG) (Invitrogen) were used as the secondary antibodies. The sections were mounted with FluorSave containing 2 $\mu g \cdot mL^{-1}$ 4′,6-diamino-2-phenylindole (DAPI), and observed under a fluorescence microscope (IX-70; Olympus, Tokyo, Japan) or confocal laser scanning microscope (FV1000; Olympus).

Immunoelectron microscopy

Ultrathin cryosections were prepared from mouse lenses as previously described [38]. In brief, mouse lenses were fixed with 4% paraformaldehyde, washed with 0.1 M NaCl/P_i containing 0.02 M glycine, and embedded in 12% gelatin in 0.1 M phosphate buffer (pH 7.4). Small blocks were incubated overnight at 4 °C in 0.1 M phosphate buffer containing 2.3 M sucrose, and quickly frozen in liquid nitrogen. Ultrathin sections (80 nm) were prepared with an ultracryomicrotome (UC6/FC6; Leica Camera AG, Solms, Germany), picked up with a 1 : 1 mixture of 2% aqueous methylcellulose and 2.3 M sucrose, and transferred to a nickel grid carrying a carbon-coated Formvar supporting film. The sections were rinsed with NaCl/P_i containing 0.02 M glycine, treated with 1% BSA in NaCl/P_i, and incubated overnight with biotinylated hamster anti-(mouse DLAD) (0.2 $\mu g \cdot \mu L^{-1}$) and 10-fold diluted rat anti-(mouse Lamp-1) (clone 1D4B). The sections were incubated at room temperature for 1 h with 5 nm colloidal gold particle-conjugated streptavidin and 10 nm colloidal gold particle-conjugated goat anti-(rat IgG) (British Biocell International, Cardiff, UK). The stained sections were fixed with 1% glutaraldehyde in NaCl/P_i, embedded in 2% methylcellulose containing 0.4% uranyl acetate (pH 4.0), air-dried, and observed with a Hitachi H-7100 electron microscope (Hitachi, Tokyo, Japan). Control staining was carried out without first antibodies.

Northern hybridization and real-time PCR

Total RNA was prepared using an RNeasy Mini Kit (Qiagen, Hilden, Germany), separated on a 1.5% agarose gel containing 2% (w/v) formaldehyde, and transferred to a nylon membrane (Roche Diagnostic). Dioxigenin (DIG)-labeled RNA probes were prepared with a DIG RNA Labeling Kit (Roche Diagnostic), and hybridization was done at 68 °C in DIG Easy Hyb (Roche Diagnostic), following the manufacturer's instructions. After washing at 68 °C in 0.1 × NaCl/Cit, the hybridized probes were detected with alkaline phosphatase-conjugated anti-DIG and the CDP-Star system (Roche Diagnostic).

For real-time PCR, RNA was reverse-transcribed using Superscript III reverse transcriptase (Invitrogen) with oligo$(dT)_{12-18}$ primers (Invitrogen). PCR was carried out using a LightCycler (Roche Diagnostic) in a reaction mixture containing LightCycler FastStart DNA Master SYBER green I (Roche Diagnostic). The amount of specific RNA was quantified when the LightCycler System detected the upstroke of the exponential phase of PCR amplification. As an external DNA standard, a cDNA of each gene was cloned into pGEM-T Easy Vector (Promega, Madison, WI). As an internal control, the expression level of β-actin mRNA was determined by real-time PCR. Primers used for the real-time PCR were as follows: DLAD, 5′-CCA

GTTCATGGCTATGAGTAC and 5′-TTAGGTCTCCAA TGCAGGTCCAGCGATTTG; crystallin γD, 5′-CTTCCA GGGCCGCCACTATGA and 5′-GAAATCCATGACTCT CCTCAG; filensin, 5′-TGTTCACAGAACGGGAAGTGG and 5′-AGGTTTTCGATCTGCTCGTTGT; E-cadherin, 5′-TGCTGCTCCTACTGTTTCTACGGA and 5′-CGAA CACCAACAGAGAGTCGTAAGG; and β-actin, 5′-TGT GATGGTGGGAATGGGTCAG and 5′-TTTGATGTCAC GCACGATTTCC.

Gene array analysis

Poly(A) RNA was selected using an mRNA Purification Kit (GE Healthcare Bioscience, Uppsala, Sweden). Gene array analysis was carried out as a custom order by Kurabo Inc. using a Uniset Mouse 20K Codelink Bioarray (GE Healthcare Bioscience), which displays probe DNAs for about 20 000 mouse genes/expressed sequence tags. In brief, double-stranded cDNA was prepared with RNA from epithelial and fiber cells of the eye lens, and transcribed *in vitro* using biotin-labeled dUTP as a substrate. The complementary RNA was used as a probe for hybridizing the array, and the hybridized RNA was detected with Cy5-conjugated streptavidin. The arrays were scanned using an arrayWoRx Biochip Reader (Applied Precision, Issaquah, WC), and the array image was analyzed using CODELINK system software (GE Healthcare). The complete dataset was submitted to the NCBI GEO (Gene Expression Omnibus) database (accession number GSE7533).

Acknowledgements

We thank M. Fujii and M. Harayama for secretarial assistance. This work was supported in part by Grants-in-Aid from the Ministry of Education, Sports and Culture in Japan.

References

1 McAvoy JW, Chamberlain CG, de Iongh RU, Hales AM & Lovicu FJ (1999) Lens development. *Eye* **13**, 425–437.
2 Piatigorsky J (1981) Lens differentiation in vertebrates. A review of cellular and molecular features. *Differentiation* **19**, 134–153.
3 Bassnett S (2002) Lens organelle degradation. *Exp Eye Res* **74**, 1–6.
4 Dahm R (1999) Lens fibre cell differentiation – a link with apoptosis? *Ophthalmic Res* **31**, 163–183.
5 van Leyen K, Duvoisin RM, Engelhardt H & Wiedmann M (1998) A function for lipoxygenase in programmed organelle degradation. *Nature* **395**, 392–395.
6 Walton J & McAvoy J (1984) Sequential structural response of lens epithelium to retina-conditioned medium. *Exp Eye Res* **39**, 217–229.
7 Vrensen GF, Graw J & De Wolf A (1991) Nuclear breakdown during terminal differentiation of primary lens fibres in mice: a transmission electron microscopic study. *Exp Eye Res* **52**, 647–659.
8 Shiokawa D & Tanuma S (1999) DLAD, a novel mammalian divalent cation-independent endonuclease with homology to DNase II. *Nucleic Acids Res* **27**, 4083–4089.
9 Krieser RJ, MacLea KS, Park JP & Eastman A (2001) The cloning, genomic structure, localization, and expression of human deoxyribonuclease IIbeta. *Gene* **269**, 205–216.
10 Shiokawa D & Tanuma SI (2001) Isolation and characterization of the DLAD/Dlad genes, which lie head-to-head with the genes for urate oxidase. *Biochem Biophys Res Commun* **288**, 1119–1128.
11 Yasuda T, Takeshita H, Iida R, Nakajima T, Hosomi O, Nakashima Y & Kishi K (1998) Molecular cloning of the cDNA encoding human deoxyribonuclease II. *J Biol Chem* **273**, 2610–2616.
12 Evans CJ & Aguilera RJ (2003) DNase II: genes, enzymes and function. *Gene* **322**, 1–15.
13 Kawane K, Fukuyama H, Kondoh G, Takeda J, Ohsawa Y, Uchiyama Y & Nagata S (2001) Requirement of DNase II for definitive erythropoiesis in the mouse fetal liver. *Science* **292**, 1546–1549.
14 Kawane K, Fukuyama H, Yoshida H, Nagase H, Ohsawa Y, Uchiyama Y, Iida T, Okada K & Nagata S (2003) Impaired thymic development in mouse embryos deficient in apoptotic DNA degradation. *Nat Immunol* **4**, 138–144.
15 Nishimoto S, Kawane K, Watanabe-Fukunaga R, Fukuyama H, Ohsawa Y, Uchiyama Y, Hashida N, Ohguro N, Tano Y, Morimoto T *et al.* (2003) Nuclear cataract caused by a lack of DNA degradation in the mouse eye lens. *Nature* **424**, 1071–1074.
16 Cheng YC, Hsueh CC, Lu SC & Liao TH (2006) Identification of three crucial histidine residues (His115, His132 and His297) in porcine deoxyribonuclease II. *Biochem J* **398**, 177–185.
17 MacLea KS, Krieser RJ & Eastman A (2003) Structural requirements of human DNase II alpha for formation of the active enzyme: the role of the signal peptide, N-glycosylation, and disulphide bridging. *Biochem J* **371**, 867–876.
18 Wang CC, Lu SC, Chen HL & Liao TH (1998) Porcine spleen deoxyribonuclease II. Covalent structure, cDNA sequence, molecular cloning, and gene expression. *J Biol Chem* **273**, 17192–17198.
19 Baker KP, Baron WF, Henzel WJ & Spencer SA (1998) Molecular cloning and characterization of human and murine DNase II. *Gene* **215**, 281–289.

20 Hawse JR, DeAmicis-Tress C, Cowell TL & Kantorow M (2005) Identification of global gene expression differences between human lens epithelial and cortical fiber cells reveals specific genes and their associated pathways important for specialized lens cell functions. *Mol Vis* **11**, 274–283.
21 Halbleib JM & Nelson WJ (2006) Cadherins in development: cell adhesion, sorting, and tissue morphogenesis. *Genes Dev* **20**, 3199–3214.
22 Bassnett S & Mataic D (1997) Chromatin degradation in differentiating fiber cells of the eye lens. *J Cell Biol* **137**, 37–49.
23 Foley JD, Rosenbaum H & Griep AE (2004) Temporal regulation of VEID-7-amino-4-trifluoromethylcoumarin cleavage activity and caspase-6 correlates with organelle loss during lens development. *J Biol Chem* **279**, 32142–32150.
24 Ishizaki Y, Jacobson MD & Raff MC (1998) A role for caspases in lens fiber differentiation. *J Cell Biol* **140**, 153–158.
25 Weber GF & Menko AS (2005) The canonical intrinsic mitochondrial death pathway has a non-apoptotic role in signaling lens cell differentiation. *J Biol Chem* **280**, 22135–22145.
26 Nagata S (2005) DNA degradation in development and programmed cell death. *Annu Rev Immunol* **23**, 853–875.
27 Zandy AJ, Lakhani S, Zheng T, Flavell RA & Bassnett S (2005) Role of the executioner caspases during lens development. *J Biol Chem* **280**, 30263–30272.
28 van Leyen K, Duvoisin RM, Engelhardt H & Wiedmann M (1998) A function for lipoxygenase in programmed organelle degradation. *Nature* **395**, 391–395.
29 Bleich D, Chen S, Zipser B, Sun D, Funk CD & Nadler JL (1999) Resistance to type 1 diabetes induction in 12-lipoxygenase knockout mice. *J Clin Invest* **103**, 1431–1436.
30 Klein RF, Allard J, Avnur Z, Nikolcheva T, Rotstein D, Carlos AS, Shea M, Waters RV, Belknap JK, Peltz G *et al.* (2004) Regulation of bone mass in mice by the lipoxygenase gene Alox15. *Science* **303**, 229–232.
31 Medina-Martinez O, Brownell I, Amaya-Manzanares F, Hu Q, Behringer RR & Jamrich M (2005) Severe defects in proliferation and differentiation of lens cells in Foxe3 null mice. *Mol Cell Biol* **25**, 8854–8863.
32 Daniels R, Rusan NM, Wadsworth P & Hebert DN (2006) SV40 VP2 and VP3 insertion into ER membranes is controlled by the capsid protein VP1: implications for DNA translocation out of the ER. *Mol Cell* **24**, 955–966.
33 Tanida I, Tanida-Miyake E, Komatsu M, Ueno T & Kominami E (2002) Human Apg3p/Aut1p homologue is an authentic E2 enzyme for multiple substrates, GATE-16, GABARAP, and MAP-LC3, and facilitates the conjugation of hApg12p to hApg5p. *J Biol Chem* **277**, 13739–13744.
34 Kingma PB, Bok D & Ong DE (1998) Bovine epidermal fatty acid-binding protein: determination of ligand specificity and cellular localization in retina and testis. *Biochemistry* **37**, 3250–3257.
35 Matsui M, Yamamoto A, Kuma A, Ohsumi Y & Mizushima N (2006) Organelle degradation during the lens and erythroid differentiation is independent of autophagy. *Biochem Biophys Res Commun* **339**, 485–489.
36 Murai K, Murakami H & Nagata S (1998) Myeloid-specific transcriptional activation by murine myeloid zinc finger protein-2. *Proc Natl Acad Sci USA* **95**, 3461–3466.
37 Ray S & Diamond B (1994) Generation of a fusion partner to sample the repertoire of splenic B cells destined for apoptosis. *Proc Natl Acad Sci USA* **91**, 5548–5551.
38 Koike M, Nakanishi H, Saftig P, Ezaki J, Isahara K, Ohsawa Y, Schulz-Schaeffer W, Watanabe T, Waguri S, Kametaka S *et al.* (2000) Cathepsin D deficiency induces lysosomal storage with ceroid lipofuscin in mouse CNS neurons. *J Neurosci* **20**, 6898–6906.

Critical role of the p400/mDomino chromatin-remodeling ATPase in embryonic hematopoiesis

Takeshi Ueda[1,3], Rie Watanabe-Fukunaga[1,3], Hironori Ogawa[1,3], Hidehiro Fukuyama[1], Yujiro Higashi[2], Shigekazu Nagata[1,3] and Rikiro Fukunaga[1,3,*]

[1]*Laboratory of Genetics (B-3), and* [2]*Developmental Biology Laboratory, Graduate School of Frontier Biosciences and Graduate School of Medicine, Osaka University, 2-2 Yamadaoka, Suita, Osaka 565-0871, Japan*

[3]*Solution-Oriented Research for Science and Technology, Japan Science and Technology Corporation, 2-2 Yamadaoka, Suita, Osaka 565-0871, Japan*

The SWI2/SNF2 family ATPase, p400/mDomino, is a core subunit of a large chromatin-remodeling complex, and is currently suggested to play a unique function in histone variant exchange, a process by which chromatin structure is altered. Here, we investigated the role of p400/mDomino in mammalian development by generating mutant mice with a targeted deletion of the N-terminal domain of p400/mDomino (referred to as mDom$^{\Delta N/\Delta N}$). The mDom$^{\Delta N/\Delta N}$ mice died on embryonic day 11.5 (E11.5), and displayed an anemic appearance and slight deformity of the neural tube. DNA microarray and quantitative RT-PCR analyses revealed that all of the embryonic globin genes and a globin chaperone gene were poorly expressed in the mDom$^{\Delta N/\Delta N}$ embryo and yolk sac on E8.5, indicating that primitive erythropoiesis was impaired. A hematopoietic colony assay indicated that the hematopoietic activity of the yolk sac was significantly blocked in the mutant mice. We also found that the expression of a limited set of Hox genes, including Hoxa7, Hoxa9 and Hoxb9, was drastically enhanced in the mDom$^{\Delta N/\Delta N}$ yolk sacs. These results suggest that p400/mDomino plays a critical role in embryonic hematopoiesis by regulating the expression of developmentally essential genes such as those in the Hox gene cluster.

Introduction

The alteration of chromatin structure is a critical process for the transcriptional activation or repression of various cell-type-specific or developmentally regulated genes, and is executed principally by two types of enzymatic activities, covalent histone modification and non-covalent but ATP-hydrolysis-dependent chromatin remodeling. All of the ATP-dependent chromatin remodelers are multisubunit protein complexes containing a SWI2/SNF2 family DNA-dependent ATPase subunit, which plays a central role in the remodeling machinery's alteration of the structure, composition and positioning of nucleosomes. Based on the structural similarity of the core ATPase domain and other domain motifs in the ATPase subunit, the remodelers have been divided into five distinct classes: SWI/SNF, ISWI, Mi-2/CHD, INO80 and SWR1 (Cairns 2005; van Attikum & Gasser 2005; de la Serna *et al.* 2006; Saha *et al.* 2006). Numerous studies on the ATP-dependent chromatin remodelers in yeast, *Drosophila*, and mammals have demonstrated that they have diverse biological functions in gene expression, DNA repair and recombination, cellular proliferation and differentiation, and the development of multicellular organisms (van Attikum & Gasser 2005; de la Serna *et al.* 2006; Saha *et al.* 2006).

p400/mammalian Domino (p400/mDomino, Gene symbol: Ep400) is an Swr1-class DNA-dependent ATPase that was identified as a component of a novel adenovirus E1A-binding complex (Fuchs *et al.* 2001), and as an interaction partner for a myeloid-specific transcription factor, MZF-2 A (Ogawa *et al.* 2003a,b). The human and mouse p400/mDomino proteins contain a bipartite SWI2/SNF2-type ATPase domain, a SANT (*S*WI3, *A*DA2, *N*CoR and *T*FIIIB) domain, an HSA (*h*elicase- and *S*ANT-*a*ssociated) domain and a glutamine-rich domain, and are highly homologous to the *Drosophila* Domino A protein and distantly related to the *C. elegans* ssl-1 and yeast Swr1 proteins (Fuchs *et al.* 2001; Ruhf *et al.* 2001;

Communicated by: Tadashi Yamamoto
**Correspondence*: E-mail: fukunaga@genetic.med.osaka-u.ac.jp

DOI: 10.1111/j.1365-2443.2007.01080.x

Ogawa *et al.* 2003b; Ceol & Horvitz 2004; Kobor *et al.* 2004). The p400/mDomino-containing protein complex consists of more than ten subunits, including the Tip60 histone acetyltransferase and a PI3K family protein kinase TRRAP, and closely resembles the *Drosophila* dTip60 complex, which contains Domino A, dTip60 and dTra1 (Fuchs *et al.* 2001; Cai *et al.* 2005; Jin *et al.* 2005). Interestingly, this metazoan Tip60-Domino complex seems to correspond to a homologous merge of the yeast SWR1 complex and the NuA4 histone acetyltransferase complex (Doyon & Cote 2004; Cai *et al.* 2005; Jin *et al.* 2005). Another mammalian Swr1-class ATPase, SRCAP, is also known to form a multisubunit complex, which shares some components with the Tip60-mDomino complex but does not contain Tip60, suggesting a functional difference between p400/mDomino and SRCAP (Cai *et al.* 2005; Eissenberg *et al.* 2005; Jin *et al.* 2005; Ruhl *et al.* 2006).

Recent genetic and biochemical studies have demonstrated that the yeast and *Drosophila* SWR1-class complexes execute a unique remodeling function, called histone variant exchange. The *Saccharomyces cerevisiae* SWR1 complex associates with Htz1 protein, a histone variant categorized as H2A.Z, and is essential for the deposition of Htz1 into chromatin via its ATP-dependent catalytic activity, thereby replacing histone H2A with Htz1 in nucleosomal arrays (Krogan *et al.* 2003, 2004; Kobor *et al.* 2004; Mizuguchi *et al.* 2004). On the other hand, the *Drosophila* dTip60-Domino complex possesses activities to acetylate the phosphorylated form of the H2Av histone variant, and to subsequently exchange it with unmodified H2Av in nucleosomal arrays (Kusch *et al.* 2004). Thus, these SWR1-class remodelers are responsible for the regulated deposition of selective histone H2A variants into nucleosomes, which probably plays essential roles in the epigenetic regulation of gene expression as well as in DNA repair (Jin *et al.* 2005; Sarma & Reinberg 2005; van Attikum & Gasser 2005). Functional studies using mammalian cultured cell lines have shown that p400/mDomino is involved in the expression of genes that are regulated by transcription factors such as c-Myc, MZF-2 A and E2F (Frank *et al.* 2003; Ogawa *et al.* 2003b; Taubert *et al.* 2004), and plays significant roles in p53/p21-dependent cellular senescence, in E1A-mediated transformation, and in E1A- or DNA damage-induced apoptosis (Fuchs *et al.* 2001; Chan *et al.* 2005; Samuelson *et al.* 2005; Tyteca *et al.* 2006). Together, these findings suggest that p400/mDomino functions in various biological processes through its role in chromatin remodeling activities. However, its physiological roles in mammalian development and organogenesis remain unknown.

Here, we report that the targeted mutation of p400/mDomino in mice caused early embryonic lethality with profound defects in yolk sac hematopoiesis. The expressions of embryonic globin genes and a globin chaperone gene were markedly reduced in the mDomino-mutated embryos, whereas the expressions of a set of Hox genes were drastically increased, suggesting a critical role for p400/mDomino in the epigenetic regulation of developmentally controlled genes. Intriguingly, *Drosophila* Domino is essential for the development of fly blood cells, hemocytes, and *domino* mutations show a genetic interaction with Polycomb group (PcG) and Trithorax group (TrxG) genes, the epigenetic regulators for homeotic gene expression (Braun *et al.* 1997, 1998; Ruhf *et al.* 2001). These findings may indicate that the mammalian and *Drosophila* Tip60-mDomino complexes play conserved roles in the development of analogous tissues, via their chromatin-remodeling activities.

Results

Generation of mDomino-targeted mice

The targeting constructs for the mouse mDomino gene are shown in Fig. 1A. The 1.56 kb region from the *Kpn*I site in exon 2 to the *Hin*dIII site in intron 2 of the p400/mDomino gene was replaced with a neomycin-resistance gene cassette (Neo). Mouse embryonic stem (ES) cell clones containing the mDomino-targeted allele were identified by PCR (not shown) and Southern blot analyses (Fig. 1B), and used to generate gene-targeted mice. Although we had designed the targeting vector with the aim of generating mDomino-null mice, this construct resulted in expression of an N-terminally truncated protein of mDomino, as described below. Thus, we named the mutated allele as $mDom^{\Delta N}$. Mice heterozygous for the mutated allele ($mDom^{+/\Delta N}$) were crossed to generate homozygotes, but the genotypic analysis of 121 pups showed 53 wild-type mice, 68 heterozygotes and no homozygotes (Table 1), suggesting that the homozygous mutation was embryonically lethal. Characterization of the mutant embryos through development showed that the homozygous embryos ($mDom^{\Delta N/\Delta N}$) were developmentally arrested around embryonic day 9.5 (E9.5), and no mutants were found viable beyond E11.5 (Table 1). Since $mDom^{+/\Delta N}$ mice were phenotypically normal and fertile, the truncated mDomino protein was unlikely to behave as a dominant-negative mutant.

Ubiquitous expression of mDomino in early embryos

Since the lethality of $mDom^{\Delta N/\Delta N}$ mice *in utero* suggested that mDomino plays a critical role in early embryogenesis,

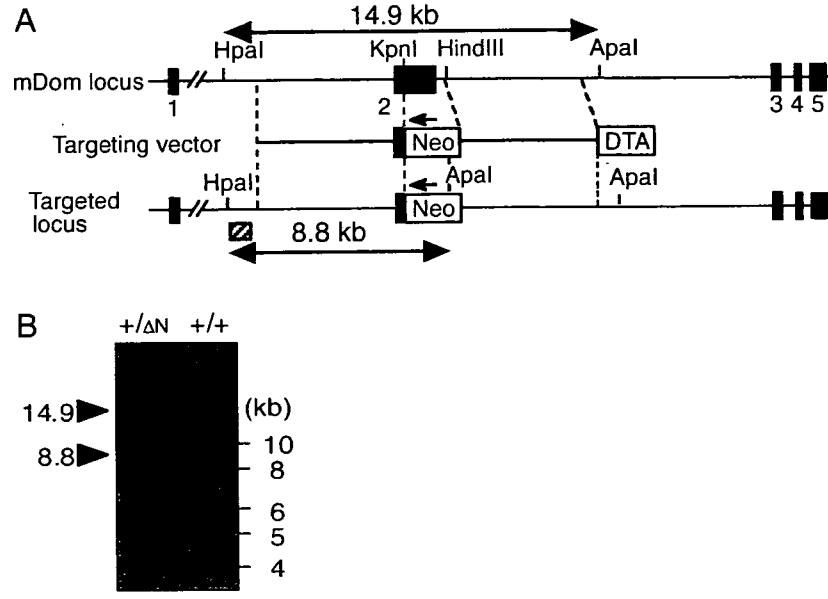

Figure 1 Targeted disruption of the mouse p400/mDomino gene. (A) Schematic illustration of the exon organization of the mDomino gene and targeting strategy. The exons of the mDomino gene are indicated by filled boxes. The targeting vector was designed to replace exon 2 with a Neo^R cassette (Neo). The DTA gene used for negative selection was placed at the end of the 3′ homologous arm. A probe used for Southern blot analysis is indicated by a hatched box. (B) Southern blot analysis of the genomic DNA from $mDom^{+/\Delta N}$ and wild-type mice. DNA was digested with *ApaI* and *HpaI*, and analyzed by Southern hybridization. As indicated in panel A, the wild-type and targeted alleles of the mDomino gene were predicted to result in 14.9 and 8.8 kb bands, respectively.

Table 1 Genotype analysis of progeny from mDom heterozygous matings

Stage	Total	+/+	+/ΔN	ΔN/ΔN
E8.5	245	78	112	55
E9.5	36	10	17	9
E10.5	23	3	11	9
E11.5	6	3	3	0
Adult	121	53	68	0

we first examined the expression of mDomino in embryos. Quantitative RT-PCR analysis revealed that the mDomino gene was expressed in both the yolk sac and embryo proper at E8.5 (data not shown), and whole mount *in situ* hybridization using an anti-sense probe of exon 2 showed ubiquitous expression of the mDomino transcript throughout the E8.5 embryo (Fig. 2A).

To characterize the mDomino gene product and its subcellular localization, we prepared mouse embryonic fibroblasts (MEFs) from wild-type, $mDom^{+/\Delta N}$ and $mDom^{\Delta N/\Delta N}$ embryos at E8.5, and analyzed them for mDomino expression by immunoblotting using antibodies specific for the N- or C-terminal region of mDomino (Ogawa *et al.* 2003b). As shown in Fig. 2B, a 350-kDa product, the predicted size of mDomino, was detected with the anti-Dom-N and anti-Dom-C antibodies in the extracts from wild-type and $mDom^{+/\Delta N}$ MEFs but not in those from $mDom^{\Delta N/\Delta N}$ MEFs. On the other hand, a smaller product (~300 kDa) was detected by the anti-Dom-C antibody in the $mDom^{+/\Delta N}$ and $mDom^{\Delta N/\Delta N}$ extracts. This product was not recognized by the anti-N antibody, and appeared to be a truncated mDomino protein lacking the large N-terminal region encoded by exon 2. To test this, we analyzed RNAs from the wild-type and mDom-targeted MEFs by RT-PCR using primer sets specific for regions between exon 1 and exon 3, 4 or 5 of the mDomino gene, and found that an aberrant mDomino mRNA produced by splicing between exons 1 and 3, which was undetectable in wild-type MEFs, was significantly expressed in $mDom^{\Delta N/\Delta N}$ and $mDom^{+/\Delta N}$ MEFs (data not shown). Thus, the targeted replacement of exon 2 with the neo cassette happened to result in expression of the aberrant mDomino mRNA, which was likely to be translated from an internal ATG codon in exon 3 to produce the mutant protein lacking the N-terminal 471 amino acids. The apparent molecular mass (~300 kDa) of the small product in Fig. 2B was consistent with the calculated molecular mass (282.9 kDa) of the predicted mutant protein.

Immunofluorescence analysis of these MEFs using the anti-Dom-N and anti-Dom-C antibodies showed nuclear staining of both wild-type and $mDom^{\Delta N/\Delta N}$ cells, indicating that the truncation of the N-terminal domain did not change the nuclear localization of mDomino protein (Fig. 2C). In the nucleus, mDomino was detected as granular dots that were excluded from nucleoli, as shown by fibrillarin staining, and from the DAPI-dense heterochromatic region (Fig. 2D).

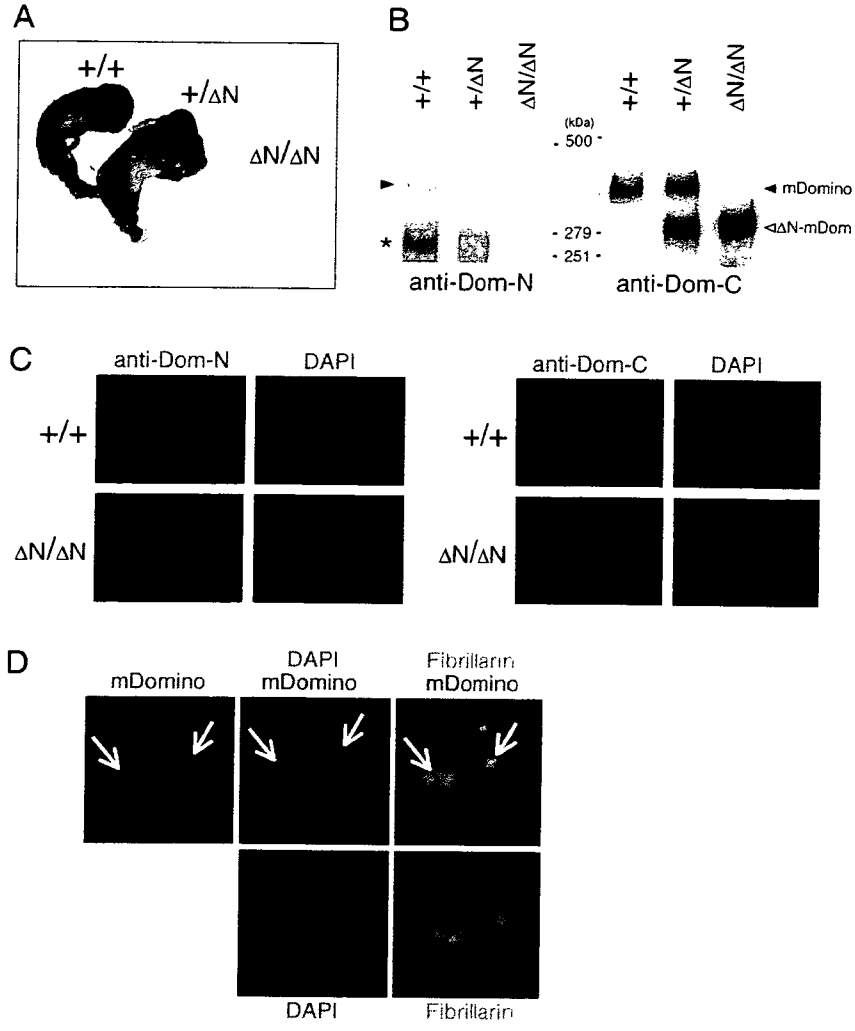

Figure 2 p400/mDomino expression in E8.5 embryos and embryonic fibroblasts. (A) Expression of the mDomino transcript in E8.5 embryos was assessed by whole mount *in situ* hybridization using a specific anti-sense probe for exon2. The absence of a hybridization signal in the mDom$^{\Delta N/\Delta N}$ embryo confirmed the specificity of the probe. (B) Expression of the mDomino protein in embryonic fibroblasts prepared from mDom$^{+/+}$, mDom$^{+/\Delta N}$ and mDom $^{\Delta N/\Delta N}$ E8.5 embryos. Whole-cell extracts were analyzed by immunoblotting with an anti-Dom-N or anti-Dom-C antibody as described in Experimental procedures. The asterisk indicates a nonspecific signal. (C) Immunofluorescence analyses for the wild-type and truncated mDomino proteins in embryonic fibroblasts. Cells were stained with the anti-Dom-N or anti-Dom-C antibody (red) as described in Experimental procedures. Nuclei were visualized by DAPI (blue) staining. (D) Wild-type embryonic fibroblasts were stained with the anti-Dom-N antibody (red), DAPI (blue), and an antibody specific for the nucleolar marker protein fibrillarin (green). Merged images show that mDomino was not co-localized with either the nucleoli or the DAPI-dense loci in the nucleus, as indicated by arrows.

Reduced expression of erythroid-specific genes in mDom$^{\Delta N/\Delta N}$ embryos

Although the mDom$^{\Delta N/\Delta N}$ embryos displayed a grossly anemic appearance, enlarged pericardial sacs and growth retardation around E9.5–10.5 (Fig. 3A), the mutant embryos at E8.5 were morphologically indistinguishable from their wild-type littermates, except they displayed a wavy neural tube (Figs 2A and 3B). Hematoxylin–eosin staining of sections of the developing neural tube did not reveal evident histological abnormalities that would explain the slight deformity of the neural tube (data not shown). To characterize the neural tube formation of the mutant embryos, we examined the expression of several genes in E8.5 embryos by whole mount *in situ* hybridization. However, this analysis revealed that neuroepithelial or somite marker genes, such as Pax6, Lunatic-fringe, Sox2, Patched, Ngn2, Mash1, Fgf8, Necab, Id1 and Id3, were expressed in similar patterns in the wild-type, mDom$^{+/\Delta N}$ and mDom$^{\Delta N/\Delta N}$ embryos (Fig. 3B, and data not shown).

Therefore, to explore the genes affected by the mDomino mutation systematically, we examined the gene expression profile at E8.5 of wild-type and mDom$^{\Delta N/\Delta N}$ embryos using DNA microarrays consisting of about 36 000 mouse genes. Comparative analysis of the wild-type and mDom$^{\Delta N/\Delta N}$ embryos (GEO accession number: GSE5358) revealed that the expression of ~40 genes was significantly reduced in the mDom$^{\Delta N/\Delta N}$ E8.5 embryos (with a normalized signal intensity of wild-type > 5.0, and signal intensity ratio of wild-type to mDom$^{\Delta N/\Delta N}$ greater than twofold), of which 17 genes showed a > 2.5-fold difference (Table 2). Although seven of the genes were functionally unannotated, the array analysis revealed that the expression of the embryonic globin genes Hba-x, Hbb-y and Hbb-bh1 was much lower (4%–21% of the wild-type levels) in the mDom$^{\Delta N/\Delta N}$ embryos. The

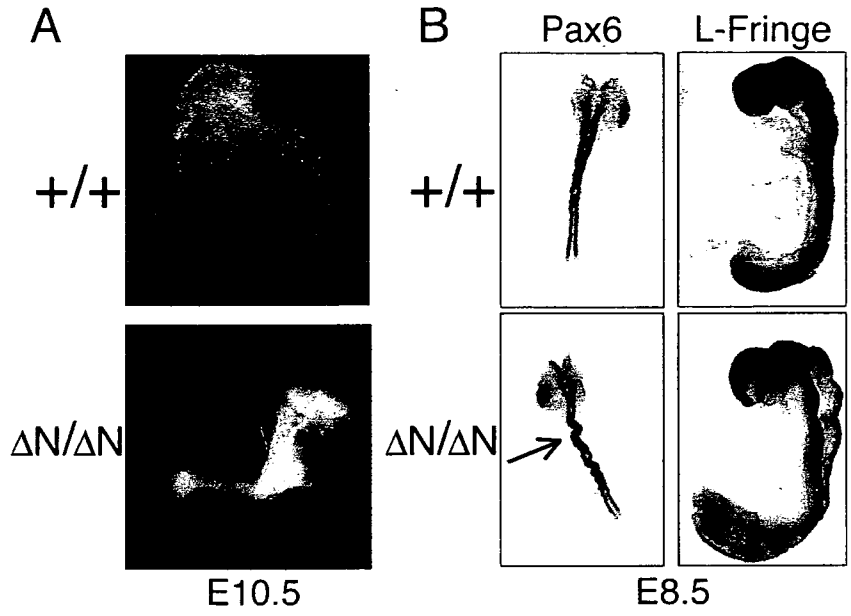

Figure 3 Morphological abnormality of mDomino-mutated embryos. (A) Lateral view of E10.5 wild-type and mutant embryos. (B) Whole-mount *in situ* hybridization analyses of E8.5 embryos for expression of the Pax6 and Lunatic fringe genes. The wavy neural tube in the mDom$^{\Delta N/\Delta N}$ embryo is indicated by an arrow.

Table 2 DNA microarray analysis of genes affected by mDomino mutation in E8.5 embryos

Product	Wild-type signal	Mutant signal	W/M ratio	Accession number
IMAGE cDNA clone: 6815954	16.86	0.03	664.60	BC059042.1
IMAGE cDNA clone: 4221423	44.05	0.20	225.13	BF780346.1
RIKEN cDNA clone: 4921522H04	18.83	0.34	55.32	AV255740.2
Hemoglobin Y, β-like embryonic chain (Hbb-y)	140.55	5.36	26.20	NM_008221.2
IMAGE cDNA clone: 517329	28.08	1.33	21.13	AI596639.1
IMAGE cDNA clone: 3411884	16.92	1.60	10.57	BE691298.1
Hemoglobin X, α-like embryonic chain (Hba-x)	209.92	23.53	8.92	NM_010405.2
α Hemoglobin stabilizing protein (AHSP)	21.44	3.94	5.45	NM_133245.1
Hemoglobin Z, β-like embryonic chain (Hbb-bh1)*	118.48	24.33	4.87	BF608957.1
Hemoglobin Z, β-like embryonic chain (Hbb-bh1)*	292.94	60.84	4.82	BF608957.1
Hemoglobin α, adult chain 1 (Hba-a1)	163.59	35.73	4.58	AA208349.1
Zic family member 1 (Zic1)	11.86	3.55	3.34	NM_009573.2
Ring finger protein 110 (Rnf110)	13.74	4.17	3.29	NM_009545.1
Phosphatidylethanolamine binding protein (Pebp)	85.72	27.30	3.04	BM949026.1
RIKEN cDNA clone: 5730469D23	41.44	13.26	3.13	AK017687.1
RIKEN cDNA clone: 9630027M08	7.06	2.36	3.00	AK079334.1
Myosin, light polypeptide 2, regulatory, cardiac, slow	20.60	7.17	2.87	NM_010861.1
Forkhead box D1 (Foxd1)	8.32	3.22	2.59	NM_008242.1

Normalized signal intensities were presented for the wild-type and mutant embryos.
*Results obtained with two different probes.

gene expression of Hba-a1, which is expressed in both embryonic and adult erythrocytes in mice (Fantoni *et al.* 1981), and of an erythrocyte-specific globin chaperone protein, AHSP (α-hemoglobin stabilizing protein) (Kihm *et al.* 2002), was also reduced in the mDom$^{\Delta N/\Delta N}$ embryos. These results suggest that genes critical for primitive erythrocytes were impaired in the mDom$^{\Delta N/\Delta N}$ embryos.

A reduced expression of the Zic1, Foxd1 and Rnf110 genes in the mutant embryos was also detected (Table 2). Zic1 and Foxd1 are zinc finger- and forkhead box-transcription factors, respectively, and are implicated in early neurogenesis (Herrera *et al.* 2004; Grinberg & Millen 2005). Rnf110 (Ring finger protein 110, also known as Mel-18, Zfp144 or Pcgf2) is a member of the mammalian

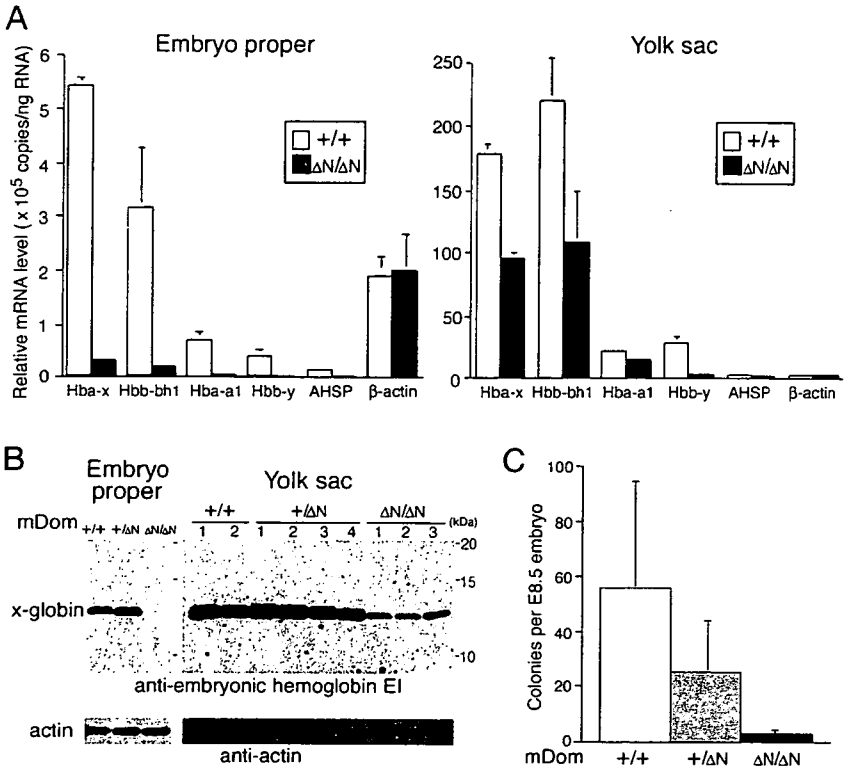

Figure 4 Defects in primitive hematopoiesis in mDom$^{\Delta N/\Delta N}$ embryos. (A) Expression levels of mRNAs for the embryonic globins, AHSP and β-actin in wild-type and mDom$^{\Delta N/\Delta N}$ embryos proper (left) and yolk sacs (right) were quantified by real-time RT-PCR, and the averages of the results from two independent experiments are shown. (B) Protein levels of the embryonic x-globin chain. Whole-cell extracts were prepared from the individual embryo proper (left) or yolk sac (right) from littermate-matched E8.5 embryos and analyzed by immunoblotting using a rabbit anti-mouse embryonic hemoglobin EI antibody. The filters were re-blotted with an anti-actin antibody as a loading control. (C) E8.5 embryos were used for a hematopoietic colony formation assay as described in Experimental procedures. Colonies containing more than 30 cells were counted after 10 days of culture, and the average number of colonies per embryo is presented with error bars showing the standard deviation. Wild-type, $n = 5$; mDom$^{+/\Delta N}$, $n = 7$; mDom$^{\Delta N/\Delta N}$, $n = 5$.

PcG genes, which are homologous to *Drosophila Posterior sex combs*, and is known to play roles in the regulation of Hox gene expression (Akasaka *et al.* 2001). Thus, the expression of various genes involved in early embryogenesis appeared to be impaired by the mDomino mutation. We could not identify genes that were significantly up-regulated in the mDom$^{\Delta N/\Delta N}$ embryos compared with the wild-type embryos by the DNA array analysis.

Critical role of mDomino in early embryonic hematopoiesis

To confirm the results of the DNA array analysis, we performed quantitative, real-time RT-PCR using the total RNA from E8.5 embryos. Consistent with the microarray data, the embryonic globin and AHSP genes were abundantly expressed in the wild-type embryos, but their mRNA levels were much lower (< 10% of the wild-type level) in the mDom$^{\Delta N/\Delta N}$ embryos (Fig. 4A, left). We also examined the expression of these genes in the yolk sac, since the hematopoietic events begin in the extra-embryonic blood islands of the yolk sac at E7.0 and the yolk sac hematopoiesis still dominates at the E8.5 stage (Dzierzak *et al.* 1998). The mRNA levels of the erythroid-specific genes in the mDom$^{\Delta N/\Delta N}$ yolk sac at E8.5 were about 15%–50% of the levels in the wild-type yolk sac (Fig. 4A, right). To examine the protein levels of the embryonic globins, we performed an immunoblot analysis of the E8.5 embryo proper and yolk sac using a rabbit anti-mouse embryonic hemoglobin EI (x 2y2) polyclonal antibody, which recognizes both the embryonic x-globin (encoded by Hba-x) and y-globin (encoded by Hbb-y) chains (Miwa *et al.* 1991), with strong preference for the x-globin chain (our unpublished observation). The immunoblot analysis demonstrated that the protein level of x-globin was dramatically lower than wild-type in the mDom$^{\Delta N/\Delta N}$ embryo proper (Fig. 4B, left), and significantly lower in the mDom$^{\Delta N/\Delta N}$ yolk sac, although to a lesser extent (Fig. 4B, right). These results suggest that the mDomino mutation impaired the primitive erythropoiesis that occurs in the yolk sac, which in turn resulted in a lack of blood cells in the embryo proper. The severe reduction of globin levels in the mDom$^{\Delta N/\Delta N}$ embryo proper in comparison with the yolk sac may be partly due to inefficient supply of erythrocytes through the nascent allantoic vasculature, although the chorio-allantoic fusion seemed to occur at E8.5 (6–8 somite pairs) without apparent morphological abnormality (data not shown).

Although the reduced expression of embryonic globin genes reflected the impaired production of primitive erythrocytes, it was not clear whether the hematopoietic activity of the progenitor cells in the yolk sac was affected

by the mDomino mutation. To address this issue, we performed a hematopoietic colony formation assay. After 10 days in methylcellulose culture, the yolk sac cells from mDom$^{+/+}$ and mDom$^{+/\Delta N}$ E8.5 embryos generated dozens of hematopoietic colonies, whereas the mDom$^{\Delta N/\Delta N}$ yolk sac cells yielded only a few colonies (Fig. 4C). DAF staining of the resulting colonies showed that the majority of the colonies arising from the mDom$^{+/+}$ and $^{+/\Delta N}$ yolk sacs consisted mostly of hemoglobin-positive erythroid cells (74% and 66%, respectively). The mDom$^{\Delta N/\Delta N}$ colonies, although the colony number was reduced, contained the same proportion of erythroid colonies (67%). This result suggests that there is a cell-autonomous defect in the yolk sac hematopoietic precursors in the mDom$^{\Delta N/\Delta N}$ embryos.

The mDomino mutation enhances the expression of Hox genes in the yolk sac

Previous studies suggested that the *Drosophila domino* gene has a repressive function on homeotic genes via interactions with PcG and TrxG genes (Ruhf *et al.* 2001). A mammalian homologue of *Drosophila trithorax*, mixed-lineage leukemia (MLL), is known to positively regulate the expression of a set of Hox genes, including Hoxa7 and a9, which appear to play important roles in MLL-dependent leukemogenesis and hematopoiesis (Hess *et al.* 1997; Yu *et al.* 1998; Ayton & Cleary 2003; Ernst *et al.* 2004; Milne *et al.* 2005). These observations prompted us to examine whether the mDomino mutation could perturb the expression of these Hox genes in early embryos. When compared with the wild-type yolk sac, the mDom$^{\Delta N/\Delta N}$ yolk sac displayed a markedly increased expression of the Hoxa7 and Hoxa9 genes (eight- and tenfold, respectively), while the mDom$^{\Delta N/\Delta N}$ embryo proper showed comparable to or slightly lower expressions of these genes than the wild-type embryo proper (Fig. 5A). The expression levels of other genes in the HoxA locus (Hoxa4, a5, a6 and a10) were comparable between the mDom$^{+/+}$ and mDom$^{\Delta N/\Delta N}$ yolk sacs (Fig. 5B) and embryos proper (data not shown). We further examined the expression of paralogous genes in other Hox clusters, and found a drastic increase in Hoxb9 expression in the mutant yolk sacs (Fig. 5B). The expression levels of other paralogous genes (Hoxb6, b7, b8, c8, c9 and d8) were comparable between the wild-type and mutant yolk sacs (Fig. 5B, and data not shown). The expression levels of the β-actin gene (Fig. 4A) and hematopoietic marker genes Scl, Lmo2 and GATA2 (data not shown) were comparable in the wild-type and mutant yolk sacs. These results indicate that the mDomino mutation resulted in the mis-expression or de-repression of only a certain set of Hox genes in the yolk sac cells.

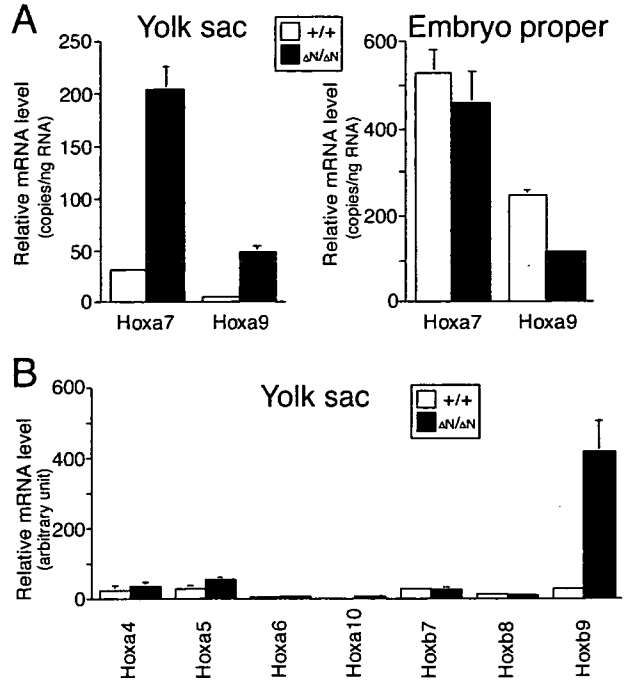

Figure 5 Elevated expression of Hoxa7, Hoxa9 and Hoxb9 genes in the mDom$^{\Delta N/\Delta N}$ yolk sac. (A) Expression of the Hoxa7 and Hoxa9 genes in the wild-type and mDom$^{\Delta N/\Delta N}$ yolk sac and embryo proper was measured by real-time RT-PCR. (B) Expression of the indicated Hox genes in the yolk sac was measured by real-time RT-PCR, and is presented as the relative mRNA level in arbitrary units as described in Experimental procedures.

Discussion

Gene targeting studies have demonstrated that distinct classes of the SWI2/SNF2 family of DNA-dependent ATPases play critical roles in embryonic development and hematopoiesis (de la Serna *et al.* 2006). For example, mice deficient in the SWI/SNF-class ATPase Brg1 show embryonic lethality at the peri-implantation stage (Bultman *et al.* 2000), and mice with a hypomorphic Brg1 mutation develop normally until mid-gestation but then exhibit defective erythropoiesis, and eventual anemia and lethality around E12.5 (Bultman *et al.* 2005). Mice deficient in the ISWI-class ATPase SNF2h also show early embryonic lethality (~E7.5), and the anti-sense knockdown of SNF2h expression in human bone marrow progenitors inhibits cytokine-dependent erythropoiesis *in vitro* (Stopka & Skoultchi 2003).

In this report, we generated mutant mice of an SWR1-class ATPase p400/mDomino, which exhibited embryonic lethality around E9.5. The aberrant splicing of the transcript from the targeted gene resulted in the expression of the N-terminally truncated mDomino

protein. Although we have not succeeded in determining whether the truncated protein is active in the chromatin-remodeling function, it still contains the entire regions of the HSA, ATPase, SANT and glutamine-rich domains, suggesting that the truncated mDomino is likely to retain at least the DNA-dependent ATPase/helicase activity. Thus, we note that the phenotypes observed here would reflect hypomorphic properties of this mutant but not those of the null mutation. It was unlikely that the ΔN-mDomino behaved as a dominant-negative mutant, since no apparent phenotype was observed in the heterozygous mice.

Although the $mDom^{\Delta N/\Delta N}$ E8.5 embryos did not show apparent morphological abnormality except for a slight deformity of the neural tube, DNA microarray and quantitative RT-PCR analyses revealed that the expression of embryonic globin genes was reduced in the $mDom^{\Delta N/\Delta N}$ embryos proper and yolk sacs. Consistent with this observation, the hematopoietic colony-forming activity was severely impaired in the $mDom^{\Delta N/\Delta N}$ yolk sac. These results indicate that mDomino plays a critical role in primitive hematopoiesis in the yolk sac. It is widely known that mid-gestation lethal phenotypes accompanied with hematopoietic defects shown by gene-knockout mice are often attributed to placental insufficiency. However, since our analyses of the mDom mutant mice were performed at E8.5 (5–12 somite pairs), the decrease in primitive hematopoiesis is likely due to the intrinsic defect in proliferating and/or differentiating ability of the hematopoietic progenitors in the yolk sac, although we cannot exclude a possibility that a functional defect of the nascent chorio-allantoic placenta caused the more severe reduction of $mDom^{\Delta N/\Delta N}$ erythroid cells in the embryo proper than in the yolk sac. The hematopoietic phenotype of the $mDom^{\Delta N/\Delta N}$ mice may reflect a functional conservation of homologous genes in mammalian and fly development. The *Drosophila domino* gene was originally identified as a loss-of-function mutation characterized by the total absence of circulating hemocytes, the blood cells for innate immunity in *Drosophila* (Braun *et al.* 1997, 1998), and was later shown to be required for cellular viability and proliferation in developing tissues as well as for oogenesis (Ruhf *et al.* 2001).

Cued by the genetic interaction between the domino gene and PcG/TrxG genes in *Drosophila* (Ruhf *et al.* 2001), we investigated Hox gene expression in the mutant mice, and found that a subset of Hox genes, Hoxa7, Hoxa9 and Hoxb9, were over-expressed in the $mDom^{\Delta N/\Delta N}$ yolk sacs. Ectopic expression or de-repression of these Hox genes has been observed in mice lacking mammalian PcG genes such as Bmi-1 and Mel-18 (Hanson *et al.* 1999; Akasaka *et al.* 2001; Cao *et al.* 2005), whereas Hox gene silencing has been demonstrated in cells from MLL-deficient mice (Yu *et al.* 1998; Hanson *et al.* 1999; Ernst *et al.* 2004). Recent studies demonstrated that MLL specifically associates with a subset of its target loci, including the Hoxa7 and Hoxa9 genes (Milne *et al.* 2005). In this context, mDomino is likely to play a role in controlling Hox gene expression in the yolk sac, where mDomino would function cooperatively with PcG gene products and/or antagonistically with MLL. This hypothesis is consistent with the function of *Drosophila* domino, which has a repressive effect on homeotic gene expression via an enhancing interaction with PcG genes and an opposing interaction with TrxG members (Ruhf *et al.* 2001). A physical association of p400/mDomino with Enhancer of Polycomb (EPc) in a large nuclear complex (Fuchs *et al.* 2001; Cai *et al.* 2005) supports this idea. MLL is a histone methyltransferase specific for histone H3-Lys4, whose methylation is positively related to active gene expression and the maintenance of this expression (Milne *et al.* 2005). In contrast, two Polycomb repressive complexes (PRCs), PRC2 and PRC1, possess distinct histone-modifying activities for H3-Lys27 methylation and H2A-Lys119 monoubiquitylation, respectively, both of which appear to play essential roles in gene silencing and the maintenance of this silenced state (Cao *et al.* 2005; Martin & Zhang 2005). Therefore, the p400/mDomino chromatin remodeling complex may play a role in linking the TrxG/PcG-mediated histone modifications with the ATP-dependent histone variant exchange for the alternation and/or maintenance of chromatin organization, although we have no experimental evidence for this hypothesis.

The molecular mechanism by which p400/mDomino regulates embryonic hematopoiesis remains unknown, but accumulating evidence suggests that the strictly regulated expression of Hox cluster genes by MLL and PcG members is essential for mammalian hematopoiesis, and a malfunction of MLL or PcG causes hematopoietic disorders such as leukemia/lymphoma or progenitor reduction. MLL-deficient hematopoietic progenitors exhibit a marked reduction in their ability to proliferate and differentiate, which is rescued by the expression of a range of Hox genes (Hess *et al.* 1997; Ernst *et al.* 2004). On the other hand, the Bmi-1 and Rae28 PcG genes are required for the proliferative potential, self-renewal and maintenance of hematopoietic stem cells (van der Lugt *et al.* 1994; Ohta *et al.* 2002; Lessard & Sauvageau 2003; Park *et al.* 2003; Iwama *et al.* 2004; Kim *et al.* 2004). Although the increased expression of the limited set of Hox genes cannot be simply correlated with the hematopoietic defects observed in the yolk sac of $mDom^{\Delta N/\Delta N}$ mice, the dysregulated Hox gene expression may contribute, at least in part, to the impaired yolk sac hematopoiesis.

Our studies have shown that mDomino is ubiquitously expressed in early embryos and adult tissues (Ogawa *et al.* 2003b), and its mutation seems to affect not only primitive hematopoiesis but also neural tube formation and cardiac development. Although a detailed investigation of $mDom^{\Delta N/\Delta N}$ mice in later developmental stages is hampered by the embryonic lethality, future studies using mice with null mutation or conditional gene-targeted mice would help to elucidate the physiological roles of mDomino in definitive hematopoiesis and the development of other tissues and organs.

Experimental procedures

Construction of targeting vectors, and the generation and genotyping of mutant mice

To construct the targeting vector, a neomycin-resistance gene (Neo cassette) was inserted between the *KpnI* site in exon 2 and the *Hin*dIII site in intron 2 of the mouse mDomino gene, cloned from a mouse 129/Sv genomic DNA library. The diphtheria toxin A fragment gene (DTA cassette) for negative selection was ligated to the 3′ end of the 3′ homologous arm (Fig. 1A). Production of $mDom^{+/\Delta N}$ mice was performed as described (Ueda *et al.* 2004). In brief, mouse R1 ES cells were transfected with the targeting vector by electroporation, and G418-resistant clones were screened for homologous recombination by PCR. ES clones carrying the single mDomino-targeted allele were injected into BDF1 blastocysts, which were then implanted into recipient ICR female mice. Chimeric mice with a high ES contribution were crossed to C57BL/6 females to yield $mDom^{+/\Delta N}$ mice. Germ-line transmission was identified by coat color and then confirmed by PCR. mDomino heterozygotes were intercrossed to generate homozygous mutants. All mice were housed in a specific pathogen-free facility at Osaka University Medical School and all animal experiments were carried out in accordance with protocols approved by the Osaka University Medical School Animal Care and Use Committee (Osaka, Japan).

Genomic DNA for PCR was prepared from tail snips from infant mice or the yolk sacs from embryos. The genotype of the mDomino locus was determined by polymerase chain reaction (PCR) using a mixture of three specific primers: mDom-2S (5′-AGA-ATGTCCAACATCAGCTGCAGAGGTCTA-3′), mDom-2AS (5′-ATCATGTTTCCCTGTAGATGTTGCAAGAAG-3′) and NeoR (5′-GATTCGCAGCGCATCGCCTTCTATCG-3′) as described (Ueda *et al.* 2004). The amplified bands corresponding to the wild-type and mutated alleles of the mDomino gene were 1.18 and 0.7 kb in length, respectively. Southern hybridization analysis was performed as described (Ueda *et al.* 2004).

Whole mount *in situ* hybridization

Mouse embryos were isolated and fixed in 4% paraformaldehyde overnight at 4 °C, dehydrated in a graded ethanol series, and then used for the procedure. Whole mount *in situ* hybridization of the E8.5 embryos was performed using digoxigenin-labeled probes and color development with NBT (Nitro blue tetrazolium chloride)/BCIP (5-Bromo-4-chloro-3-indolyl phosphate, toluidine salt), as described (Maruhashi *et al.* 2005). The 993-bp *Rsa*I fragment (235–1227, corresponding to a region in exon 2) of the mDomino cDNA was cloned in pBluescript II SK + and used for preparing the anti-sense probe. The RNA probes were prepared by transcription of the linearized plasmid with T3 or T7 RNA polymerase (Promega), using digoxigenin-11-UTP (Roche). After hybridization and color development, the embryos were observed with a stereomicroscope (Stemi DV4, Zeiss).

Preparation of mouse embryonic fibroblasts (MEFs)

Embryo-derived fibroblasts were prepared from E8.5 embryo proper as described (Xu *et al.* 1999), with some modifications. Briefly, E8.5 embryos from heterozygous breeding pairs were dissected from the decidual tissue and isolated from the yolk sac, and then transferred to individual wells in a 24-well tissue culture plate. Each embryo was trypsinized, dissected by pipetting and cultured in medium containing high-glucose DMEM (Invitrogen), 30% FCS (Invitrogen) and 50 μM 2-mercaptoethanol in a new tissue culture plate. Confluent cells were passaged in the same medium containing 10% FCS.

Immunoblot and immunofluorescence analyses

For the detection of endogenous mDomino protein, MEFs were lyzed directly in Laemmli's sample loading buffer and heated for 30 min at 85 °C and for 5 min at 95 °C. The samples were separated by electrophoresis on a 7.5% SDS-polyacrylamide gel and transferred to a polyvinylidene difluoride membrane filter (Millipore). Immunoblot analysis was carried out using the enhanced chemiluminescence system (Perkin-Elmer) with rabbit anti-Dom-N or anti-Dom-C polyclonal antibody (Ogawa *et al.* 2003b) and peroxidase-conjugated goat anti-rabbit immunoglobulin (Dako). For the detection of the embryonic globin proteins, each embryo proper or yolk sac from litter-matched embryos at E8.5 was lyzed as described above. The lysates were separated by electrophoresis on a 15%–25% SDS-polyacrylamide gel, and analyzed by immunoblotting using rabbit anti-mouse embryonic hemoglobin EI polyclonal antibody (a kind gift from Dr Tadao Atsumi) (Miwa *et al.* 1991). As a loading control, the membranes were reblotted with an anti-actin monoclonal antibody (clone C4, MP Biomedicals).

For immunofluorescence staining, cells cultured in four-well slide chambers (#154526, Nalgene Nunc) were fixed with 4% paraformaldehyde for 10 min, permeabilized with phosphate-buffered saline (PBS) containing 0.2% Triton X-100 for 20 min at room temperature, blocked with PBS containing 5% skim milk for 30 min, and then incubated with the affinity-purified anti-Dom-N antibody and mouse anti-fibrillarin monoclonal antibody (Upstate Biotechnology) for 60 min at 37 °C. The samples were then washed with PBS, and incubated with the Alexa Fluor 488-conjugated anti-mouse IgG antibody (Invitrogen) and Cy3-conjugated anti-rabbit IgG antibody (Jackson ImmunoResearch Laboratories), for 30 min at 37 °C. The nuclei were counterstained with DAPI, and cells were observed by fluorescence microscopy.

Gene array analysis

Gene array analysis was performed as a 'custom order' by Kurabo with a CodeLink Mouse Whole Genome Bioarray (GE Healthcare Bio-Sciences), which displays probe DNAs for about 36 000 mouse genes and expressed sequence tags. Total RNA was prepared from litter-matched embryos at E8.5 ($mDom^{+/+}$, $n = 42$; $mDom^{\Delta N/\Delta N}$, $n = 45$) using the RNeasy extraction kit (QIAGEN). Double-stranded cDNA was then prepared from the RNA and was transcribed *in vitro* with biotin-labeled UTP as a substrate. The complementary RNA was used as a probe for hybridization of the array, and the hybridized RNA was detected with Cy5-conjugated streptavidin. The arrays were scanned using a Biochip Reader (Applied Precision), and the array image was analyzed with CODELINK SYSTEM Software (GE Healthcare Bio-Sciences).

Real-time reverse transcriptase-PCR (RT-PCR) for quantitative analysis of mRNA

Total RNA was prepared from litter-matched embryos proper ($mDom^{+/+}$, $n = 42$; $mDom^{\Delta N/\Delta N}$, $n = 45$) and yolk sacs ($mDom^{+/+}$, $n = 8$; $mDom^{\Delta N/\Delta N}$, $n = 10$), as described above. Single-stranded cDNA was synthesized from the total RNA (0.5 μg) using an oligo-(dT) primer and Superscript III (Invitrogen). Real-time RT-PCR analysis was carried out using the LightCyclerFastStart DNA Master SYBR Green I kit (Roche), as described (Iida *et al.* 2005), under the following conditions: 40 cycles of 15 s at 95 °C, 5 s at 62 °C and 20 s at 72 °C. The primer sets used for the real-time RT-PCR were listed in Supplementary Table S1. The specific amplification of each targeted cDNA was confirmed by melting temperature analysis and by the presence of a single PCR product on agarose gel electrophoresis. In all real-time RT-PCR experiments except for Fig. 5B, cloned cDNA fragments (10^2–10^8 copies per reaction) containing the respective target region were amplified in parallel and used as standards, and the sample data were normalized against the standards and expressed as copy numbers of target mRNA per nanogram of total RNA. In the experiments in Fig. 5B, the sample data were normalized against the β-actin standard curve, and were expressed as relative mRNA levels in arbitrary units, where the mRNA level of β-actin was defined as 10^6 units.

Hematopoietic colony assay

E8.5 embryos including the yolk sac from wild-type, $mDom^{+/\Delta N}$ and $mDom^{\Delta N/\Delta N}$ littermates were treated with PBS containing 20% FCS and 0.1% collagenase D (Roche) at 37 °C for 60 min, and passed through 27-gauge needles to obtain single-cell suspensions. The cells were washed with PBS containing 20% FCS and then plated in 1% methylcellulose/Iscove's MDM containing 15% FCS, 10 μg/mL insulin, 200 μg/mL transferrin, 50 ng/mL stem cell factor (SCF), 10 ng/mL IL-3, 10 ng/mL IL-6 and 3 units/mL erythropoietin (MethoCult M3434, Stem Cell Technologies). Colonies containing more than 30 cells were counted after 10 days of culture. Erythroid colonies were stained with DAF (2,7-diaminofluorene) (Wako), as described (Worthington *et al.* 1987).

Acknowledgements

We are grateful to Dr Tadao Atsumi for the anti-mouse embryonic hemoglobin EI antibody. We also thank Drs Kohki Kawane and Mitsuji Maruhashi for help in the analysis of the mutant mice. This work was supported in part by Grants-in-Aid from the Ministry of Education, Culture, Sports, Science and Technology of Japan.

References

Akasaka, T., van Lohuizen, M., van der Lugt, N., Mizutani-Koseki, Y., Kanno, M., Taniguchi, M., Vidal, M., Alkema, M., Berns, A. & Koseki, H. (2001) Mice doubly deficient for the Polycomb Group genes Mel18 and Bmi1 reveal synergy and requirement for maintenance but not initiation of Hox gene expression. *Development* **128**, 1587–1597.

van Attikum, H. & Gasser, S.M. (2005) The histone code at DNA breaks: a guide to repair? *Nat. Rev. Mol. Cell Biol.* **6**, 757–765.

Ayton, P.M. & Cleary, M.L. (2003) Transformation of myeloid progenitors by MLL oncoproteins is dependent on Hoxa7 and Hoxa9. *Genes Dev.* **17**, 2298–2307.

Braun, A., Hoffmann, J.A. & Meister, M. (1998) Analysis of the *Drosophila* host defense in domino mutant larvae, which are devoid of hemocytes. *Proc. Natl. Acad. Sci. USA* **95**, 14337–14342.

Braun, A., Lemaitre, B., Lanot, R., Zachary, D. & Meister, M. (1997) *Drosophila* immunity: analysis of larval hemocytes by P-element-mediated enhancer trap. *Genetics* **147**, 623–634.

Bultman, S.J., Gebuhr, T.C. & Magnuson, T. (2005) A Brg1 mutation that uncouples ATPase activity from chromatin remodeling reveals an essential role for SWI/SNF-related complexes in β-globin expression and erythroid development. *Genes Dev.* **19**, 2849–2861.

Bultman, S., Gebuhr, T., Yee, D., La Mantia, C., Nicholson, J., Gilliam, A., Randazzo, F., Metzger, D., Chambon, P., Crabtree, G. & Magnuson, T. (2000) A Brg1 null mutation in the mouse reveals functional differences among mammalian SWI/SNF complexes. *Mol. Cell* **6**, 1287–1295.

Cai, Y., Jin, J., Florens, L., Swanson, S.K., Kusch, T., Li, B., Workman, J.L., Washburn, M.P., Conaway, R.C. & Conaway, J.W. (2005) The mammalian YL1 protein is a shared subunit of the TRRAP/TIP60 histone acetyltransferase and SRCAP complexes. *J. Biol. Chem.* **280**, 13665–13670.

Cairns, B.R. (2005) Chromatin remodeling complexes: strength in diversity, precision through specialization. *Curr. Opin. Genet. Dev.* **15**, 185–190.

Cao, R., Tsukada, Y. & Zhang, Y. (2005) Role of Bmi-1 and Ring1A in H2A ubiquitylation and Hox gene silencing. *Mol. Cell* **20**, 845–854.

Ceol, C.J. & Horvitz, H.R. (2004) A new class of *C. elegans* synMuv genes implicates a Tip60/NuA4-like HAT complex as a negative regulator of Ras signaling. *Dev. Cell* **6**, 563–576.

Chan, H.M., Narita, M., Lowe, S.W. & Livingston, D.M. (2005) The p400 E1A-associated protein is a novel component of the p53 → p21 senescence pathway. *Genes Dev.* **19**, 196–201.

Doyon, Y. & Cote, J. (2004) The highly conserved and multifunctional NuA4 HAT complex. *Curr. Opin. Genet. Dev.* **14**, 147–154.